

# **IMPROVED 3-D SEISMIC EDGE DETECTION WITH THE MAGIC CUBE OPERATOR**

BY

**ADETOKUNBO, RASHEED PETER**

A Thesis Presented to the  
DEANSHIP OF GRADUATE STUDIES

**KING FAHD UNIVERSITY OF PETROLEUM & MINERALS**

DHAHRAN, SAUDI ARABIA

1963 ١٣٨٣

In Partial Fulfillment of the  
Requirements for the Degree of

**MASTER OF SCIENCE**

In

**GEOPHYSICS**

APRIL, 2015




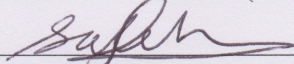
KING FAHD UNIVERSITY OF PETROLEUM & MINERALS  
DHAHRAN 31261, SAUDI ARABIA

DEANSHIP OF GRADUATE STUDIES

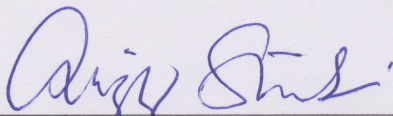
This thesis, written by **ADETOKUNBO, RASHEED PETER** under the direction of his thesis advisor and approved by his thesis committee, has been presented to and accepted by the Dean of Graduate Studies, in partial fulfillment of the requirements for the degree of **MASTER OF SCIENCE IN GEOPHYSICS**.

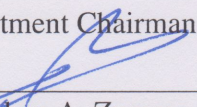
Thesis Committee

  
Dr. Abdullatif Al-Shuhail (Advisor)

  
Dr. Saleh Al-Dossary (Member)

  
Dr. Abdullah Alshuhail (Member)

  
Dr. Abdulaziz Al-Shaibani  
Department Chairman

  
Dr. Salam A. Zummo  
Dean of Graduate Studies

  
Date



©Adetokunbo, Rasheed Peter  
2015

## *Dedication*

*To my lovely parents and siblings for their prayers and support.*



# ACKNOWLEDGMENTS

I want to express my heartfelt gratitude to all the people who directly or indirectly contributed to this work. Since the list of names is inexhaustible, I hereby apologize in advance, in case I miss someone in particular.

I like to express my indebtedness of gratitude to:

- **Dr. Abdullatif Al-Shuhail** for his thorough supervision of this thesis. Without his immense support, this work would not have been possible. I thank him for his idea, constructive criticism and continuing discussions throughout the course of my thesis. I appreciate you most sincerely for your trust in my capability to work on this problem.
- **Dr. Saleh Al-Dossary** on whose idea this thesis is based. I highly appreciate the opportunity to benefit from his scientific experience. He is always available to help. He also took his time to read through my thesis and provided useful corrections. I also thank him for providing the 3-D seismic data for testing my codes.
- **Dr. Abdullah Alshuhail** for his immense contributions. He painstakingly read through my thesis and provided useful corrections and suggestions.
- **Saudi Aramco** for kindly providing relevant dataset.

- **Dr. Gino Janampa Ananos and Lateef Kareem** for useful discussions and sharing Matlab programming tips.
- **Staff of the Earth Sciences Department** for their immense support and contribution towards the success of my program. Many thanks to Dr. Abdulaziz Shaibani and Dr. Ismail Kaka for their leadership and administrative role. I want to thank Prof. Gabor Korvin for his fatherly care, support and advice at all times. He is always there and ready to help his students.
- **KFUPM** for the opportunity to advance my career.
- **Saudi Arabian Government** through the Ministry of Higher Education for providing scholarship to complete my masters program.
- **Nigerian community and friends** for their support, care, advice and companionship.

Last but not least I want to thank my parents and siblings for their immense supports, care and prayers. I appreciate you for being there for me at all times.



# TABLE OF CONTENTS

	Page
<b>ACKNOWLEDGEMENTS</b>	<b>iii</b>
<b>LIST OF FIGURES</b>	<b>vii</b>
<b>ABSTRACT (ENGLISH)</b>	<b>x</b>
<b>ABSTRACT (ARABIC)</b>	<b>xii</b>
<b>CHAPTER 1 INTRODUCTION</b>	<b>1</b>
1.1 Introduction . . . . .	1
1.2 Statement of Problem . . . . .	3
1.3 Objectives . . . . .	4
1.4 Motivation of the Study . . . . .	4
1.5 Contributions of the Study . . . . .	5
1.6 Structure of the Thesis . . . . .	6
<b>CHAPTER 2 LITERATURE REVIEW</b>	<b>8</b>
2.1 General Overview . . . . .	8
2.2 Classification of Seismic Attributes . . . . .	9
2.3 Edge Detection Operators . . . . .	11
2.4 Convolution . . . . .	13
2.5 Previous Studies . . . . .	15

<b>CHAPTER 3</b>	<b>METHODOLOGY</b>	<b>21</b>
3.1	Introduction . . . . .	21
3.2	Magic Square . . . . .	22
3.2.1	Implementation of $F_1$ Magic Operator . . . . .	25
3.2.2	Implementation of $F_2$ Magic Operator . . . . .	26
3.3	Extension to 5 x 5 Magic Square . . . . .	28
3.4	Magic Cube . . . . .	30
3.5	Modified $F_2$ Magic cube Operator . . . . .	35
<b>CHAPTER 4</b>	<b>APPLICATION</b>	<b>44</b>
4.1	Data Summary . . . . .	44
4.2	Examples . . . . .	44
4.2.1	Magic Square Example . . . . .	47
4.2.2	Magic Cube Example . . . . .	58
4.3	Discussion . . . . .	65
<b>CHAPTER 5</b>	<b>CONCLUSION AND RECOMMENDATIONS</b>	<b>66</b>
5.1	Conclusion . . . . .	66
5.2	Recommendations . . . . .	68
<b>APPENDIX</b>		<b>69</b>
<b>REFERENCES</b>		<b>73</b>
<b>VITAE</b>		<b>81</b>



# LIST OF FIGURES

2.1	Seismic attributes derived from or related to the basic seismic information of time, amplitude, frequency, and attenuation (after Brown, 2001).	10
2.2	Some application of seismic attributes; (a)-(c) Original data volume and results with variance and chaos attributes (Randen et al., 2001), (d)-(f) Original time slice and results with conventional Sobel and multidirectional Sobel (Al-Dossary and Al-Garni, 2013) and (g)-(f) Original time slice and result with coherence attribute (Bahorich and Farmer, 1995)	20
3.1	Magic squares; (a) Normal magic square by Lo-Shu, (b)-(h) All 90-degree rotational and reflectional squares of Lo-Shu.	24
3.2	New kernels derived from normal magic square.	24
3.3	(a) A pixel and its adjacent neighbors sorted in ascending order, (b)-(d) Rearrangement of sorted elements in square lattice based on $M_1, M_2, M_3$ and $M_4$ .	26
3.4	Directional magic square operators or kernels ( $K$ ).	27
3.5	(a) 5 x 5 normal magic square, (b) New kernel derived from (a).	28
3.6	Directional 5 x 5 magic square operators.	29
3.7	Normal magic cube operators.	32
3.8	Seven magic cube kernels (after Al-Shuhail and Al-Dossary, 2014).	33
3.9	The corresponding edge detection kernels along with their associated directions of maximum gradient in 3-D space (after Al-Shuhail and Al-Dossary, 2014).	34

3.10	Flowchart of the procedure to construct and apply the proposed magic cube operator. . . . .	36
3.11	Eight magic cubes produced by the modified algorithm. . . . .	37
3.12	Templates derived from the eight magic cubes. . . . .	38
3.13	The corresponding 3 x 3 x 3 edge detection kernels. . . . .	39
3.14	Normal magic cube by Trump and Boyer (Boyer, 2003). . . . .	40
3.15	Normal magic cube (Andrews, 2004). . . . .	41
3.16	The corresponding 5 x 5 x 5 edge detection kernels. . . . .	42
3.17	Schematic illustration of directions scanned by the kernels (shown by the solid arrow). . . . .	43
4.1	3-D seismic volume. (X = Crossline, Y = Inline, Z = Time slice) . . . .	45
4.2	Extracted slices from the 3-D seismic volume; (a) Inline 280, (b) Crossline 310, (c) Time slice extracted at 720 ms and (d) 3-D display of these slices. . . . .	46
4.3	Gradient edge maps of the 3 x 3 magic square $F_1$ with (a) $M_1$ and (b) $M_3$ . . . .	49
4.4	Gradient edge maps of the 3 x 3 magic square $F_2$ operator along (a) North direction, (b) Northeast direction, (c) East direction and (d) Southeast direction. . . . .	50
4.5	Maximum gradient edge map of the 3 x 3 magic square $F_2$ operator. . . .	51
4.6	Gradient edge maps of the 5 x 5 magic square $F_2$ operator along (a) North direction, (b) Northeast direction, (c) East direction and (d) Southeast direction. . . . .	52
4.7	Maximum gradient edge map of the 5 x 5 magic square $F_2$ operator. . . .	53
4.8	Comparison of gradient edge maps; (a) 3 x 3 Sobel operator, (b) 3 x 3 magic square $F_1$ operator; (c) 5 x 5 Sobel operator and (d) 5 x 5 magic square $F_1$ operator. . . . .	54
4.9	Comparison of gradient edge maps; (a) 3 x 3 Sobel operator, (b) 3 x 3 magic square $F_2$ operator, (c) 5 x 5 Sobel operator and (d) 5 x 5 magic square $F_2$ operator. . . . .	55



4.10	Time slice with Gaussian noise of zero mean and 0.1 standard deviation.	56
4.11	Comparison of gradient edge maps in the presence of noise using (a) 3 x 3 magic square $F_2$ kernel and (b) 5 x 5 magic square $F_2$ kernel. The delineation of the two channels (blue and green arrows) suggests that the higher spatial dimension is better for data with noise. . . . .	57
4.12	Gradient edge maps of 3 x 3 x 3 magic cube $F_2$ operator using (a) K-5a, (b) K-6a, (c) K-7a and (d) K-8a kernels respectively. The blue and green arrows denote delineated channels. . . . .	59
4.13	Gradient edge maps; (a) Inline number 5 from 3-D seismic volume and (b) Result of the 3 x 3 x 3 magic cube $F_2$ operator with K-7a. . . . .	60
4.14	Gradient edge maps of 5 x 5 x 5 magic cube $F_2$ operator using (a) K-5b, (b) K-6b, (c) K-7b and (d) K-8b kernels respectively. . . . .	61
4.15	Gradient edge maps; (a) Inline number 5 from 3-D seismic volume and (b) Result of the 5 x 5 x 5 magic cube $F_2$ operator with K-7b. . . . .	62
4.16	Comparison of gradient edge maps of time slice 181; (a) Result of the maximum convolution of 3 x 3 x 3 magic cube $F_2$ operators, (b) Result of the maximum convolution of 5 x 5 x 5 magic cube $F_2$ operators and (c) Result of 3-D Sobel operator. . . . .	63
4.17	Comparison of amplitude gradient edge maps of inline number 5; (a) Result of the maximum convolution of 3 x 3 x 3 magic cube $F_2$ operators, (b) Result of the maximum convolution of 5 x 5 x 5 magic cube $F_2$ operators and (c) Result of 3-D Sobel operator. . . . .	64

# THESIS ABSTRACT

**NAME:** Adetokunbo, Rasheed Peter

**TITLE OF STUDY:** IMPROVED 3-D SEISMIC EDGE DETECTION WITH  
THE MAGIC CUBE OPERATOR

**MAJOR FIELD:** Geophysics

**DATE OF DEGREE:** April, 2015

*Edge detection is one of the categories of geometric seismic attributes that has the capability to delineate vital information from seismic reflection data which can be used to aid qualitative and quantitative interpretation. To characterize reservoirs with complex fault blocks, geophysicists often need to depict the edge of geologic bodies. This study evaluates a new method for geologic interpretation based on templates derived from magic squares and cubes. These are discrete differential operators that approximately calculate the spatial derivative of seismic amplitude through 2-D and 3-D convolution to locate edges and/or geological features of interest in seismic data. The new operator's mode of computation benefits from multidirectional scanning leading to efficient detection of different edge locations and their respective orientations. Testing using real seismic data containing a channel system shows good results in both 2-D and 3-*

*D cases. To evaluate the robustness of the operator, the operation was implemented in the presence of noise, the result was better with 5 x 5 magic square and 5 x 5 x 5 magic cube operators than for the operators with smaller spatial dimension. The overall results suggested better edge detection for steeply dipping events and more details compared with that of Sobel operator which suggests that the method can serve as a complementary tool to other existing seismic attributes.*

## Abstract – Arabic

تعتبر عملية تحديد الحواف واحدة من أهم المزايا الهندسية لسمات الإهتزازية التي لها القدرة علي إستنتاج معلومات جيولوجيه حقيقة من بيانات الاهتزازية الانعكاسية و يمكن إستخدامها في عمليتي التفسير النوعي والكمي. لتوصيف المكامن الصخريه ذات التراكيب التصدعية المعقدة , عادة يحتاج الجيوفيزيائيين لتحديد حواف تلك الوحدات والتراكيب الجيولوجيه.

في هذه الأطروحه تم عرض طريقة جديدة للتفسير الجيولوجي لبيانات الاهتزازية باستخدام نموذج مستنبط من المربع والمكعب السحري.

هذا النموذج عبارة عن معاملات تفاضليه منفصلة تحسب المشتقه المكانية لسعة الاهتزازية عن طريق كونفلوشن في بعدين او ثلاثة ابعاد وتستخدم في تحديد الحواف و/ أو الظواهر الجيولوجيه في بيانات الاهتزازية. هذا النموذج المستحدث في عملية الحوسبة يستخدم خاصية المسح و البحث عن التراكيب الصخريه في إتجاهات متعددة لبيانات الاهتزازية.

تم إختبار هذه المعاملات التفاضليه علي بيانات إهتزازيه حقيقية تحتوي علي إنظمة قنوات ذات بعدين و ثلاثة ابعاد , وظهرت نتائج ذات مصداقية عالية في كلتا الحالتين. لتقييم مدى كفاءة و فعالية هذه المعاملات، تم اختبار اطوال مختلفة لهذا النموذج في وجود بعض التشويش في البيانات الاهتزازيه. اظهر نموذج المربع السحري ذو ابعاد  $5 \times 5$  و نموذج المكعب السحري ذو ابعاد  $5 \times 5 \times 5$  افضل النتائج في تحديد التراكيب مقارنه بالنماذج ذات الابعاد الاصغر.

اظهرت الاطروحه بشكل عام بان هذا النموذج له القدرة علي تحديد حواف التراكيب الصخريه ذات زوايا ميلان حاده مقارنه بالنماذج المتوفرة حالياً . ويمكن مقارنتها بشكل إيجابي مع المعاملات التفاضليه/سويلى مما

يدل بأن الطريقة يمكن أن تكون بمثابة أداة مكملية لطرق تفسير التراكيب الجيولوجية لبيانات الاهتزازية المتوفرة حالياً.

# CHAPTER 1

## INTRODUCTION

### 1.1 Introduction

The demand for oil and gas has been growing because its advent has run in parallel with many industries that depend on products from petroleum. For example oil accounts for about 40 per cent of the world energy mix due to its sufficiency and low cost in many parts of the world, while gas accounts for about 23 per cent of the world economy mix<sup>1</sup>. As a result of its immense benefits to mankind, the growing need for hydrocarbon will continue and this poses a great challenge for geoscientists to find the reservoirs containing these resources.

In the past few decades exploration and production industries have utilized several complementary geophysical methods in the search for oil and gas resources. Of all methods, reflection seismology has been the most robust and widespread method of

<sup>1</sup>[http://www.opec.org/opec\\_web/en/900.htm](http://www.opec.org/opec_web/en/900.htm)



studying detailed subsurface geology since the 1930s. Seismic data with well logs integration has provided structural and stratigraphic imaging, pore-fluid estimation and lithofacies mapping for regional geological studies and in search for petroleum reservoirs (Sangree and Widmier, 1978; Bouvier et al., 1989; Jurado and Comas, 1992; Christensen and Mooney, 1995).

As hydrocarbon reservoirs become depleted coupled with exploration in more complex environments, seismic attribute analysis evolved three decades ago and has since revolutionized the traditional methods of seismic interpretation. The application of seismic attributes has led to the discovery of huge oil and gas reserves in subtle petroleum stratigraphic traps in various parts of the world (Justice et al., 1985; Hesthammer and Fossen, 1997; Ecker et al., 1998; Walls et al., 1999; Stright et al., 2009; Meldahl et al., 2001).

Hundreds of attributes have been developed over the decades including edge detection. Generally edge detection is an image processing operation which finds the most vital edges in an image. The algorithm has the capability to segment images into two or more regions by connecting broken edges into lines and boundaries. There are many edge detection algorithms such as Sobel (Sobel, 1970), Prewitt (Prewitt, 1970), Roberts (Roberts, 1963) and Canny (Canny, 1986). These algorithms along with others are routinely employed in digital image processing, pattern recognition and computer vision as well as in various stages of seismic data processing and interpretation. They

are used in seismic data analysis to extract vital but subtle structural and stratigraphic features such as channels, faults and fractures. These geologic features usually appear sparsely and are not easily detected especially in the presence of noise.

Edge detection also simplifies and enhances image data such that the amount of data to be processed and interpreted is minimized (Canny, 1986), while discarding other parts that are of less relevance to the task at hand. One of such algorithms that has been applied successfully to seismic data is the Sobel filter, which is a discrete differentiation operator that approximates the local gradient by combining derivatives of the amplitude between neighboring traces along the x, y, and z directions (Al-Dossary and Al-Garni, 2013).

## **1.2 Statement of Problem**

Petroleum explorationists are greatly interested in identifying and locating structural and stratigraphic discontinuities so as to aid proper geologic interpretation, well placement and prediction of potential reservoir performance. This information is often masked in the data, hence there is a need to transform the data to aid in locating and identifying these features and their respective orientations for optimum reservoir characterization.

## 1.3 Objectives

- Applying the magic square operator to seismic data.
- Extending the 2-D magic square operator to 3-D to find seismic features.
- Applying the method on real seismic data to test its performance relative to Sobel Filter.

## 1.4 Motivation of the Study

In recent decades the developments in edge detection have greatly contributed to the geological interpretation of seismic data. However, the limitation in directions of traditional edge detection often makes it difficult to get a clear and unbiased view of structural and stratigraphic features masked in 3-D seismic data which are oriented in directions not captured by a given attribute direction of computation. It is therefore important to develop new robust and efficient multidirectional operators that will accurately delineate 3-D seismic discontinuities which is vital in mapping lineaments and stratigraphic features such as faults, fractures and channels in the subsurface. The method developed in this study will improve the capability to detect different edge directions efficiently. This adds another perspectives by allowing the interpreter to view vertical, horizontal and directional lineaments independently in the data.

## 1.5 Contributions of the Study

The integration of seismic attribute analysis in seismic interpretation has greatly contributed to understanding the subsurface geology, and has been a major tool in characterizing reservoirs. Specifically, the benefits of this study include:

- Aiding seismic interpretation: The goal of seismic interpretation is to extract geologic information from seismic data such as reflections indicating geologic structure, stratigraphy, fluid content and all kinds of noise (random, multiple reflection, refracted energy etc.). The presence of noise could cause an interpreter to overlook prominent features critical to understand the structural and depositional environment. Moreover, manual interpretation can be tedious, time consuming and subject to human bias. Volume attributes operate on the entire data volume and are therefore unaffected by the interpreter or automatic picker bias, delineating subtle features that may not have been represented by horizon picks. The method described in this study will help either solely or in combination with other attributes to identify features such as unconformity, sequence boundary, major change in lithology, structural deformation (such as faulting), fault-to-fault relation and fault geometry. For example, knowledge of fault location is a key to understanding geological system and in turn a key for building geocellular models, and successful identification of drilling locations (Aqrawi et al., 2011). Knowledge of faulting network is also relevant in other applications such as hydrogeology, mineral exploration, geomechanics, construction and civil engineering projects and earthquake studies and prediction.

- Quality control in seismic data processing: Seismic attribute analysis can be incorporated in certain stages of data processing to meet interpreter objective. For example, data can be processed for fault mapping or stratigraphic features alone. Edge detection allows the seismic processor to carefully display and choose parameters to achieve his objectives.
- Edge detection is very applicable in potential field studies for finding the horizontal and vertical derivatives of potential field data which is a usual practice for structural analysis (Sertcelik and Kafadar, 2012).

## 1.6 Structure of the Thesis

The thesis is organized into five chapters as follows:

**Chapter 1** introduces the background of the proposed problem, the objectives of the study and the expected outcomes.

**Chapter 2** gives an overview of relevant previously published works and classification of seismic attributes. Theory of edge detection is also discussed.

In **Chapter 3**, I develop two methods of edge detection, and the underlining theory in accomplishing the objectives of the study are introduced. The magic square and magic cube algorithms which are the fundamentals or the building blocks of the method are also discussed.

**Chapter 4** is dedicated to the application of the new methods to a real data set. Real data used to test the method is also discussed. The first part of **Chapter 4** involves the implementation of the magic square (2-D) operator to a time slice from migrated

sections, while the latter part involves the application of magic cube operators to real seismic volume. The results of the new methods and Sobel operator are compared.

In **Chapter 5**, I draw conclusions from the results and suggest some recommendations for future studies.



## **CHAPTER 2**

# **LITERATURE REVIEW**

### **2.1 General Overview**

Seismic attributes can generally be defined as all seismically driven parameters. Chen and Sidney (1997) defined seismic attributes as specific measurements of geometric, kinematic, dynamic, or statistical features derived from seismic data. Since their introduction in the early 1970s, seismic attributes have become powerful interpretation tools initially employed qualitatively, and later in 1990s the quantitative analysis of seismic attributes became widely popular (Taner et al., 1994; Hellmich and Trappe, 1998). Since then, attributes have played an important role in contributing towards reservoir evaluation studies and reservoir property modeling through the calibration of derived seismic attributes with well measurements to obtain plausible geological maps.

The general objective in seismic attribute analysis is to transform seismic data to another domain entirely such as certain features of interests become more visible, con-

tinuous and mappable, and quantitatively to attempt to predict lateral reservoir property changes by integrating appropriate seismic attributes with well logs to enhance reservoir description and characterization of reservoirs between sparse wells.

## **2.2 Classification of Seismic Attributes**

Attributes can generally be classified based on the type of data available. Those computed from normal stacked and migrated data volume are called poststack attributes, while those computed from amplitude variation with offset (AVO) are called prestack attributes. Some of the classification of attributes in literature are as follows:

1. Chen and Sidney (1997)

- Horizon-based attributes which compute properties of seismic trace between picked horizons.
- Sample-based attributes where input traces are transformed to produce output traces with the same number of samples as the input.

2. Taner et al.(1994)

- Geometric Attributes which includes dip, azimuth and continuity
- Physical Attributes which includes amplitude, phase and frequency

3. Brown (2001) (Figure 2.1)

- Time, Amplitude, Frequency, Attenuation
- Poststack and Prestack

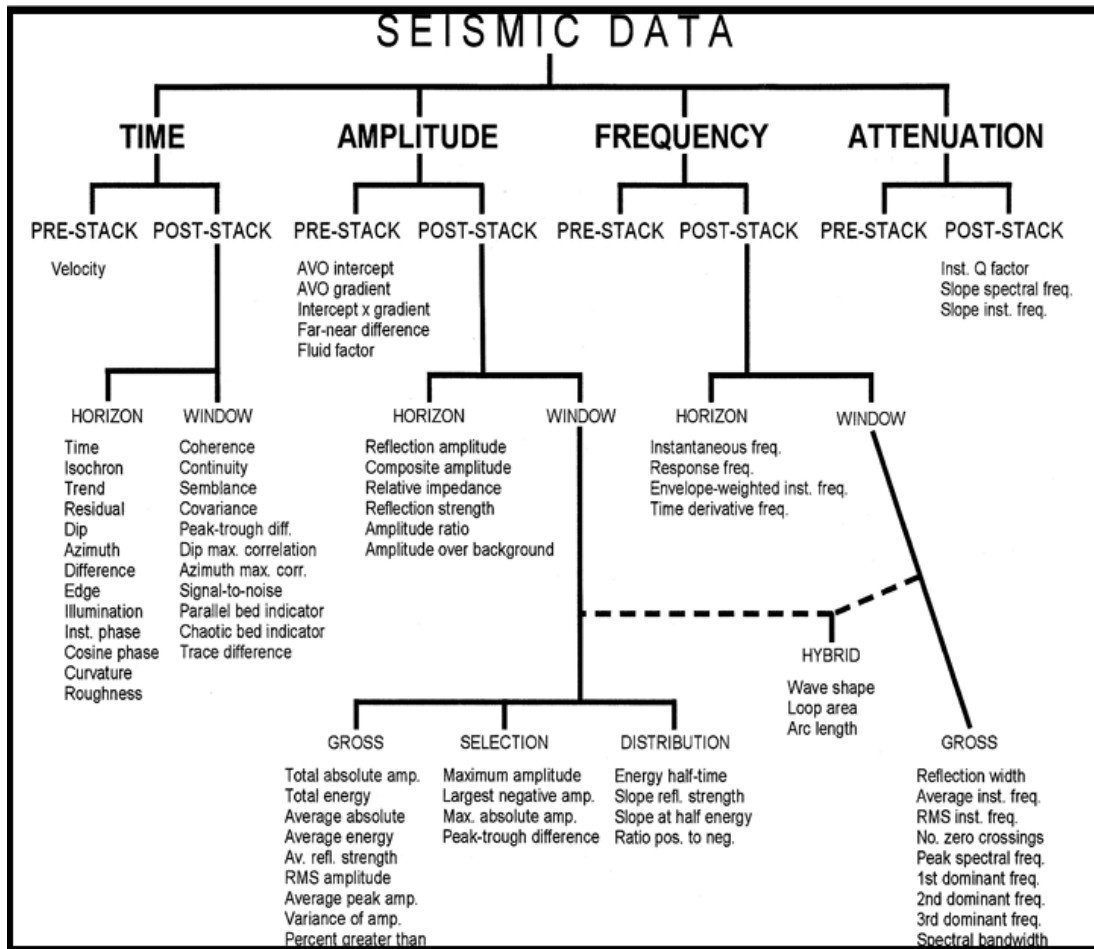


Figure 2.1: Seismic attributes derived from or related to the basic seismic information of time, amplitude, frequency, and attenuation (after Brown, 2001).

#### 4. Liner et al. (2004)

- Specific category
- General category: The list under this category includes amplitude, time, phase and frequency, complex trace, coherence, illumination, **edge detection**, AVO, spectral decomposition etc.

## 2.3 Edge Detection Operators

Edge detection methods started in 1959 (Julesz, 1959). The fundamental basis involves computing the amplitude gradient at every pixel in an input model. In some operators a threshold value is usually used as a cut-off to preserve desired gradient of the image. Over the decades several authors have developed different edge detection algorithms which can be categorized (Sharifi et al., 2002) as follows

1. Edge detection based on first derivative, e.g., Sobel (Sobel, 1970), Prewitt (Prewitt, 1970), Roberts (Roberts, 1963), Woodhall and Lindquist (1997) and so on.
2. Edge detection based on second derivative such as zero crossing (Haralick, 1984), Laplacian of Gaussian, LoG (Marr and Hildreth, 1980)
3. The Canny detection method based on certain optimal criteria (Canny, 1986)
4. The wavelet multiscale edge detection (Lee et al., 1995; Aydin et al., 1996; Christov, 2004; Sun et al., 2004)
5. Edge detection based on mathematical morphology (Matheron, 1965; Haralick et al., 1987; Matheron and Serra, 2002)
6. Edge detection method based on statistics and integral transform (Chen et al., 2011)
7. Color edge detection method (Carron and Lambert, 1994; Ruzon and Tomasi, 1999)

The first order differential operators evaluate the gradients computed along two orthogonal directions, which can be expressed by the digital discrete approximation of first-order derivative (Marques, 2011; Gonzalez and Woods, 2008) as follows:

In 2-D

$$\frac{\partial f}{\partial x} = \lim_{\Delta x \rightarrow 0} \frac{f(x + \Delta x, y) - f(x - \Delta x, y)}{2\Delta x} \quad (2.1)$$

$$\frac{\partial f}{\partial y} = \lim_{\Delta y \rightarrow 0} \frac{f(x, y + \Delta y) - f(x, y - \Delta y)}{2\Delta y} \quad (2.2)$$

In 3-D

$$\frac{\partial f}{\partial z} = \lim_{\Delta z \rightarrow 0} \frac{f(x, y, z + \Delta z) - f(x, y, z - \Delta z)}{2\Delta z} \quad (2.3)$$

where  $\frac{\partial f}{\partial x}$ ,  $\frac{\partial f}{\partial y}$  and  $\frac{\partial f}{\partial z}$  are first order partial derivatives with respect to x, y and z respectively, while  $f(x, y)$  and  $f(x, y, z)$  represents the input 2-D and 3-D data respectively.

A 3 x 3 equivalent of the first-order derivative above is the Sobel kernel which can be represented in a matrix form along the x and y directions (Sobel, 1970) as:

$$D_x = \begin{bmatrix} -1 & 0 & 1 \\ -2 & 0 & 2 \\ -1 & 0 & 1 \end{bmatrix}, \quad D_y = \begin{bmatrix} -1 & -2 & -1 \\ 0 & 0 & 0 \\ 1 & 2 & 1 \end{bmatrix} \quad (2.4)$$

The gradients along both orthogonal directions are computed by convolving  $D_x$  and  $D_y$  with the input data as:

$$\Delta_x(x, y) \approx D_x * f(x, y) \quad (2.5)$$

$$\Delta_y(x, y) \approx D_y * f(x, y) \quad (2.6)$$

At each point of an image an approximation of the gradient ( $D$ ) and angle of orientation ( $\theta$ ) in that point is computed by combining both results as follows:

$$D = \sqrt{\Delta_x^2 + \Delta_y^2} \quad (2.7)$$

$$\theta = \arctan\left(\frac{\Delta_y}{\Delta_x}\right) \quad (2.8)$$

\* means convolution operation

## 2.4 Convolution

Convolution is used in several image processing algorithms to simplify large amount of data volume since it is a spatial process which explores spatial characteristics of neighboring traces. The process is routinely carried out to achieve several objectives such as data smoothing, filtering/denoising, edge enhancement and/or edge detection using a set of predefined kernels.

Let  $F$  be an input continuous function defined on domain  $D_{m1}$ ,  $D_x$  is the convolution kernel defined on domain  $D_{m2}$ . At any given point ( $x$ ) in  $D_{m1}$ , the result is computed as



(Tertois and Frank, 2004):

$$D_x * F(x) = \int_{-\alpha}^{\alpha} D_x(a) F(x-a) \partial a \quad (2.9)$$

For each pixel at coordinates  $(x, y)$  and  $(x, y, z)$  in grid defined on domain  $D_{m1}$  of 2-D and 3-D data space respectively, equation 2.9 becomes analogously as:

$$D_x * F(x, y) = \int_{-\alpha}^{\alpha} \int_{-\alpha}^{\alpha} D_x(a, b) F(x-a, y-b) \partial a \partial b \quad (2.10)$$

$$D_x * F(x, y, z) = \int_{-\alpha}^{\alpha} \int_{-\alpha}^{\alpha} \int_{-\alpha}^{\alpha} D_x(a, b, c) F(x-a, y-b, z-c) \partial a \partial b \partial c \quad (2.11)$$

Since geological maps are presented as 2-D or 3-D images where pixel values are series of discrete numbers, we make use of discrete convolution version of equations 2.10-2.11 which are given below

$$D_x * f(x, y) = \sum_{(a,b) \in D_{m2}} D_x(a, b) f(x-a, y-b) \quad (2.12)$$

$$D_x * f(x, y, z) = \sum_{(a,b,c) \in D_{m2}} D_x(a, b, c) f(x-a, y-b, z-c) \quad (2.13)$$

where  $f(x, y)$  and  $f(x, y, z)$  are 2-D and 3-D input data respectively,  $D_{m2} = \{(a, b, c) | D_x(a, b, c) \neq 0\}$  i.e the set of all pairs  $(a, b, c)$  with non-zero value of  $D_x(a, b, c)$ .

Generally, discrete convolution performs a weighted average of all the pixels in the specified neighborhood. Intuitively, performing a discrete 2-D or 3-D convolution is

moving the convolution kernel in the data volume and computing the summation of the convolution product for each point in the grid.

There are two basic key features of convolution: linear and shift invariance. Shift invariance means that the same operation is performed for every pixel in the data grid, while linear invariance means that data points are substituted by linear combination with their neighborhood pixels.

## **2.5 Previous Studies**

Many examples related to seismic attributes and their applications to reservoir exploration and development are found in the literature. In this section I review common edge detection operators and their related geometric attributes.

Bahorich and Farmer (1995) presented the coherence attribute which gives an estimate of seismic coherence based on waveform similarity of adjacent traces from seismic amplitude in both inline and cross-line directions. The method has the capability to reveal faults as numerically separated surfaces. Subsequent algorithms (Gersztenkorn and Marfurt, 1999) based on semblance and eigenstructure provides more accurate coherence estimation than initially demonstrated. The coherence images clearly delineate buried deltas, river channels, reefs and dewatering features. The remarkable detail with which stratigraphic features show up on coherence displays, with no interpretation bias greatly aids interpretation. Skirius et al. (1999) employed

seismic coherence in North America and the Arabian Gulf to map faults and fractures in carbonates.

Al-Dossary et al. (2002) described edge preserving smoothing operator (EPS) which combines difference method and smoothing process together to achieve two objectives, namely suppressing random noise and estimating amplitude gradient. The noise suppression of the method is more robust than the conventional methods which have blurred sharp edges in their outputs. They showed some applications on synthetics, and real data from a Saudi Arabian carbonate field where amplitude gradients helped in delineating fractures.

Pepper and Van Bemmelen (2000) introduced variance cube, a measure of signal unconformity. The attribute estimates the variance in a small horizontal plane, and then smooths the results vertically. Therefore amplitude changes due to a fault will result in high variance, while amplitude changes due to non-discontinuous events will result in low variance. Variance attribute is particularly useful in mapping faults.

Iske and Randen (2005) came up with the chaos, a stratigraphic texture attribute that takes into consideration various internal configuration properties. It captures the chaotic nature of seismic signals within every 3-D window. Chaos is effective because it is invariant to amplitude, dip and azimuth. This attribute is promising in mapping channel infills, reef internal textures and gas chimneys.

Luo et al. (1996) used difference and derivative methods to process seismic data for the recognition of structural and stratigraphic discontinuities where the input data is the seismic attribute instantaneous phase. They concluded that both methods yielded high resolution edge detection capabilities, and that dip magnitude and azimuth can be used to evaluate structural forms of an area.

Lisle (1994) correlated measurement of Gaussian curvature with open fractures densities measured on outcrops. Although the exact correlation between the open fractures, paleostructure and present-day stress is not yet clearly understood, several works have demonstrated the applicability of seismic measures of reflector curvature to map hidden features. A major breakthrough in this direction is the multispectral volumetric computation of curvature by Al-Dossary and Marfurt (2006). This method measures reflector shape (reflector rotation and curvature) at various wavelengths, and is found to be complementary to the popular seismic coherence.

Al-Dossary et al. (2003) did a comparative study of Canny and Torreao and Amaral edge detection operators used in image processing to evaluate their ability to extract the full spectrum of geological features in the presence of random noise and acquisition footprint, and found Torreao and Amaral edge detector to exhibit better performance. Al-Dossary and Marfurt (2003) applied Torreao and Amarals filter that is based on Green's function to detect sharp edges and found good results since geo-

logical features like faults, fractures and channels appear as sharp edges in seismic data.

Jing et al. (2007) demonstrated the performance of the Sobel edge detector to identify boundaries of salt domes and faults, and the variation of lithological properties. Aqrabi et al. (2011) presented dip-guided 3-D Sobel to delineate clearer images of salt bodies in the Gulf of Mexico. Comparison of their results with well-known variance algorithms yielded better fault definition, more continuity and sharper salt boundary and shape. Al-Dossary and Al-Garni (2013) proposed multidirectional 3-D Sobel filter to overcome the limitation of conventional Sobel in effectively locating steeply dipping features. Song et al. (2014) developed dip guided facet model edge detector that is based on surface fitting algorithm which finds the local slope of a seismic event. This characteristic makes it better than the conventional edge detection operators that are only effective along a plane.

Pampanelli et al. (2013) presented a new edge detector called volumetric fault attribute based on first and second directional derivatives. The method proves better than variance attribute. Another advantage is that it does not enhance acquisition footprints.

Di and Gao (2014) implemented gray-level transformation and Canny edge detection for discontinuity mapping. The transformation allows the amplification of subtle local discontinuities in the presence of strong background reflections, leading to

an enhanced image for subtle faults and depositional features.

Chen and Nie (2007) developed 3 x 3 magic square templates. The method is found to be very efficient in obtaining an edge gradient map with more continuous histogram and edge direction relative to existing operators.

In this work I extend this idea into magic cubes of 3 x 3 x 3 convolution kernels similar to compass masks (e.g. Kirsch, Robinson and Frei-Chen operators) that search all directions to detect a discontinuity. Their result is comparable to 3-D Sobel operator although more tests still need to be done to validate this result.



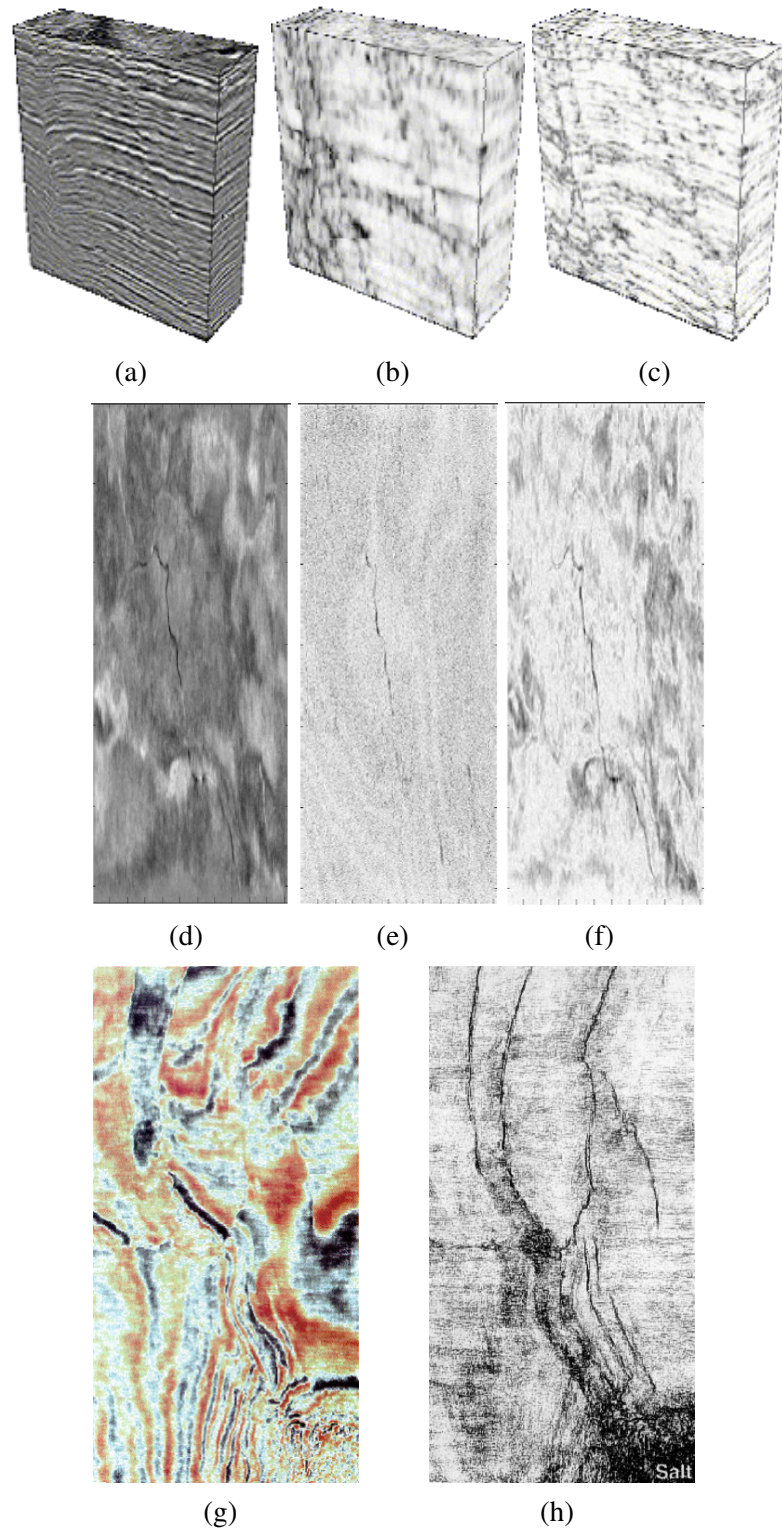


Figure 2.2: Some application of seismic attributes; (a)-(c) Original data volume and results with variance and chaos attributes (Randen et al., 2001), (d)-(f) Original time slice and results with conventional Sobel and multidirectional Sobel (Al-Dossary and Al-Garni, 2013) and (g)-(f) Original time slice and result with coherence attribute (Bahorich and Farmer, 1995)

## **CHAPTER 3**

# **METHODOLOGY**

### **3.1 Introduction**

In this section I present a new seismic edge detection method based on magic squares and cubes. The proposed method has the capability to extract seismic edge and morphological information, and the corresponding azimuths. The starting points are the magic square operators developed by Chen and Nie (2007), and its  $3 \times 3 \times 3$  magic cube extension by Al-Shuhail and Al-Dossary (2014). Both algorithms are approximate differential gradient operators similar to compass masks. I will implement their algorithms, improve them and then extend them to  $5 \times 5 \times 5$  magic square and cube operators.

The new operators will be tested using real data provided by Saudi Aramco. The performance of the operators will be tested by comparing the results obtained to those of Sobel.

## 3.2 Magic Square

Magic square has a long history in recreational mathematics (Benson and Jacoby, 1976; Ollerenshaw and Brée, 1998; Heinz and Hendricks, 2000; Semanišinová and Trenkler, 2007; Loly et al., 2009). A Magic square of order  $N$  is composed of entries  $1, 2, \dots, N^2$  or  $0, 1, \dots, N^2 - 1$  arranged in a square lattice such that the sum of all entries along the rows, columns and diagonals are equal to the magic constant of the square lattice/matrix (Heinz and Hendricks, 2000). The magic constant can be found as

$$C = \frac{N}{2}(N^2 + 1) \quad (3.1)$$

For  $N = 3$ , the magic constant is equal to 15. Figure 3.1 shows the 3 x 3 normal magic squares consisting of integers 1 – 9 constructed by rotation/reflection of one basic distinct form.

Based on the concept of magic square, Chen and Nie (2007) developed two robust edge detection operators. The operators work in a fashion similar to compass masks which search for discontinuities in all eight compass directions. Chen and Nie (2007) methods are:

- i Magic square operator based on contrast function ( $F_1$ ).
- ii Magic square operator based on discrete convolution kernel ( $F_2$ )

The two operators are based on kernels derived from a 3 x 3 magic square.  $F_1$  operator is capable of obtaining gradient map efficiently while  $F_2$  can detect both gradient or

discontinuity and edge direction. These operators take a normal magic square and rotate it clockwise by 45 degree increments in eight directions. The famous normal magic square is of the form shown in Figure 3.1a. Rotating the normal magic (or Lo-Shu) square by 45 degree increments produces seven new templates (Figures 3.1b-3.1h). A new kernel is formed by subtracting the central element from all elements of the Lo-Shu as shown in Figures 3.2a-3.2h. With each of these kernels ( $M_1$ - $M_8$ ), a contrast function ( $F_1$ ) can be built.

4	9	2	2	7	6	6	1	8	8	3	4
3	5	7	9	5	1	7	5	3	1	5	9
8	1	6	4	3	8	2	9	4	6	7	2
(a)	(b)	(c)	(d)								
4	3	8	8	1	6	6	7	2	2	9	4
9	5	1	3	5	7	1	5	9	7	5	3
2	7	6	4	9	2	8	3	4	6	1	8
(e)	(f)	(g)	(h)								

Figure 3.1: Magic squares; (a) Normal magic square by Lo-Shu, (b)-(h) All 90-degree rotational and reflectional squares of Lo-Shu.

-1	4	-3	-2	-1	4	3	-2	-1	-4	3	-2
-2	0	2	3	0	-3	-4	0	4	1	0	-1
3	-4	1	-4	1	2	1	2	-3	2	-3	4
(a) $M_1$	(b) $M_2$	(c) $M_3$	(d) $M_4$								
1	-4	3	2	1	-4	-3	2	1	4	-3	2
2	0	-2	-3	0	3	4	0	-4	-1	0	1
-3	4	-1	4	-1	-2	-1	-2	3	-2	3	-4
(e) $M_5$	(f) $M_6$	(g) $M_7$	(h) $M_8$								

Figure 3.2: New kernels derived from normal magic square.

### 3.2.1 Implementation of $F_1$ Magic Operator

Suppose the eight adjacent neighbors of any arbitrary pixel  $P$  are numbered with  $a_0, a_1, \dots, a_7$  as shown in Figure 3.3a. First the numbers around the middle pixel of interest are sorted in ascending order to obtain the sequence

$$r_{-4}, r_{-3}, \dots, r_0, \dots, r_3, r_4$$

where

$$r_{-4} < r_{-3} \dots < r_3 < r_4$$

and

$$r_i \in \{a_0, a_1, \dots, a_7\} \cup P, i = -4, -3, \dots, 3, 4$$

Using any of Figures 3.3b-d, a contrast function ( $F_1$ ) can be built as

$$\begin{aligned} F_1 = & (|(-1).r_{-1} + (-2).r_{-2} + 3.r_3| + |3.r_3 + (-4).r_{-4} + 1.r_1| + \\ & |1.r_1 + 2.r_2 + (-3).r_{-3}| + |(-3).r_{-3} + 4.r_4 + (-1).r_{-1}| + \\ & | + (-1).r_{-1} + 0.r_0 + 1.r_1| + |3.r_3 + 0.r_0 + (-3).r_{-3}| + \\ & |(-2).r_{-2} + 0.r_0 + 2.r_2| + |4.r_4 + 0.r_0 + (-4).r_{-4}|) / 8 \end{aligned} \quad (3.2)$$

$F_1$  averages eight directional edge spaces corresponding to each row, column, forward and backward diagonal leading to a good edge magnitude evaluation with good sensitivity to small changes in the gradient.

$a_0$	$a_1$	$a_2$	$r_{-1}$	$r_4$	$r_{-3}$	$r_{-2}$	$r_{-1}$	$r_4$	$r_3$	$r_{-2}$	$r_{-1}$
$a_7$	$P$	$a_3$	$r_{-2}$	$r_0$	$r_2$	$r_3$	$r_0$	$r_{-3}$	$r_{-4}$	$r_0$	$r_4$
$a_6$	$a_5$	$a_4$	$r_3$	$r_{-4}$	$r_1$	$r_{-4}$	$r_1$	$r_2$	$r_1$	$r_2$	$r_{-3}$
(a)			(b)			(c)			(d)		

Figure 3.3: (a) A pixel and its adjacent neighbors sorted in ascending order, (b)-(d) Rearrangement of sorted elements in square lattice based on  $M_1, M_2, M_3$  and  $M_4$ .

### 3.2.2 Implementation of $F_2$ Magic Operator

The second method ( $F_2$ ) utilizes a discrete convolution kernel. It is computed using the following procedure:

- i Start with any magic square aspect and subtract the central element from all elements to produce a new template.
- ii Rotate the new template by 45 degree increment to produce eight templates.
- iii Zero all elements of these templates except the absolute maxima and minima to produce the corresponding eight kernels ( $K$ ).
- iv Perform 2-D convolution of the resulting eight kernels with the 3 x 3 square centered on the point of interest in the input 2-D seismic data (D). This produces eight gradient magnitudes:  $D * K_i (i = 1, 2, \dots, 8)$ ,  $K_i$  are shown in Figure 3.4
- v The absolute maximum convolution value over the eight orientations at the point of interest is selected as the edge (E) and its kernel defines the edge direction:

$$E = \max_{i=1}^8 (D * K_i)$$

N-S Orientation	E-W Orientation	NE-SW Orientation	NW-SE Orientation																																																																																
<table> <tr><td>-1</td><td>4</td><td>0</td><td rowspan="3">N</td></tr> <tr><td>0</td><td>0</td><td>0</td></tr> <tr><td>0</td><td>-4</td><td>1</td></tr> </table> <table> <tr><td>1</td><td>-4</td><td>0</td><td rowspan="3">S</td></tr> <tr><td>0</td><td>0</td><td>0</td></tr> <tr><td>0</td><td>4</td><td>-1</td></tr> </table>	-1	4	0	N	0	0	0	0	-4	1	1	-4	0	S	0	0	0	0	4	-1	<table> <tr><td>0</td><td>0</td><td>-1</td><td rowspan="3">E</td></tr> <tr><td>-4</td><td>0</td><td>4</td></tr> <tr><td>1</td><td>0</td><td>0</td></tr> </table> <table> <tr><td>0</td><td>0</td><td>1</td><td rowspan="3">W</td></tr> <tr><td>4</td><td>0</td><td>-4</td></tr> <tr><td>-1</td><td>0</td><td>0</td></tr> </table>	0	0	-1	E	-4	0	4	1	0	0	0	0	1	W	4	0	-4	-1	0	0	<table> <tr><td>0</td><td>-1</td><td>4</td><td rowspan="3">NE</td></tr> <tr><td>0</td><td>0</td><td>0</td></tr> <tr><td>-4</td><td>1</td><td>0</td></tr> </table> <table> <tr><td>0</td><td>1</td><td>-4</td><td rowspan="3">SW</td></tr> <tr><td>0</td><td>0</td><td>0</td></tr> <tr><td>4</td><td>-1</td><td>0</td></tr> </table>	0	-1	4	NE	0	0	0	-4	1	0	0	1	-4	SW	0	0	0	4	-1	0	<table> <tr><td>-4</td><td>0</td><td>0</td><td rowspan="3">SE</td></tr> <tr><td>1</td><td>0</td><td>-1</td></tr> <tr><td>0</td><td>0</td><td>4</td></tr> </table> <table> <tr><td>4</td><td>0</td><td>0</td><td rowspan="3">NW</td></tr> <tr><td>-1</td><td>0</td><td>1</td></tr> <tr><td>0</td><td>0</td><td>-4</td></tr> </table>	-4	0	0	SE	1	0	-1	0	0	4	4	0	0	NW	-1	0	1	0	0	-4
-1	4	0	N																																																																																
0	0	0																																																																																	
0	-4	1																																																																																	
1	-4	0	S																																																																																
0	0	0																																																																																	
0	4	-1																																																																																	
0	0	-1	E																																																																																
-4	0	4																																																																																	
1	0	0																																																																																	
0	0	1	W																																																																																
4	0	-4																																																																																	
-1	0	0																																																																																	
0	-1	4	NE																																																																																
0	0	0																																																																																	
-4	1	0																																																																																	
0	1	-4	SW																																																																																
0	0	0																																																																																	
4	-1	0																																																																																	
-4	0	0	SE																																																																																
1	0	-1																																																																																	
0	0	4																																																																																	
4	0	0	NW																																																																																
-1	0	1																																																																																	
0	0	-4																																																																																	

**Legend:**  $N = North$ ,  $S = South$ ,  $E = East$ ,  $W = West$ ,  
 $NE = Northeast$ ,  $NW = Northwest$ ,  $SE = Southeast$

Figure 3.4: Directional magic square operators or kernels ( $K$ ).



Each mask responds maximally to an edge oriented in a particular direction. The orientation of the maximum edge magnitude map corresponds to the edge direction.  $F_1$  operator is highly suited for determining gradient edge map while  $F_2$  is well suited for determining gradient direction although it also provides gradient map. It should be noted that noise will compromise the efficiency of magic square operators just like other known edge detection operators.

### 3.3 Extension to 5 x 5 Magic Square

In this section I present 5 x 5 magic square  $F_1$  and  $F_2$  operators. Figure 3.5a shows an example of a normal 5 x 5 magic square and Figure 3.6 shows the corresponding kernels produced using the procedure for 3 x 3 magic square. The implementation is the same, but the difference is the spatial analysis window because 5 x 5 incorporates more neighboring pixels in both x and y directions.

17	24	1	8	15	4	11	-12	-5	2
23	5	7	14	16	10	-8	-6	1	3
4	6	13	20	22	-9	-7	0	7	9
10	12	19	21	3	-3	-1	6	8	-10
11	18	25	2	9	-2	5	12	-11	-4

(a)
(b)

Figure 3.5: (a) 5 x 5 normal magic square, (b) New kernel derived from (a).

N-S Orientation	E-W Orientation	NE-SW Orientation	NW-SE Orientation																																																																																																				
<table><tr><td>0</td><td>0</td><td>12</td><td>0</td><td>0</td></tr><tr><td>0</td><td>0</td><td>0</td><td>-1</td><td>0</td></tr><tr><td>0</td><td>0</td><td>0</td><td>0</td><td>0</td></tr><tr><td>0</td><td>1</td><td>0</td><td>0</td><td>0</td></tr><tr><td>0</td><td>0</td><td>-12</td><td>0</td><td>0</td></tr></table> <div>N</div>	0	0	12	0	0	0	0	0	-1	0	0	0	0	0	0	0	1	0	0	0	0	0	-12	0	0	<table><tr><td>0</td><td>0</td><td>0</td><td>0</td><td>0</td></tr><tr><td>0</td><td>1</td><td>0</td><td>0</td><td>0</td></tr><tr><td>-12</td><td>0</td><td>0</td><td>0</td><td>12</td></tr><tr><td>0</td><td>0</td><td>0</td><td>-1</td><td>0</td></tr><tr><td>0</td><td>0</td><td>0</td><td>0</td><td>0</td></tr></table> <div>E</div>	0	0	0	0	0	0	1	0	0	0	-12	0	0	0	12	0	0	0	-1	0	0	0	0	0	0	<table><tr><td>0</td><td>0</td><td>0</td><td>0</td><td>12</td></tr><tr><td>0</td><td>0</td><td>0</td><td>0</td><td>0</td></tr><tr><td>0</td><td>1</td><td>0</td><td>-1</td><td>0</td></tr><tr><td>0</td><td>0</td><td>0</td><td>0</td><td>0</td></tr><tr><td>-12</td><td>0</td><td>0</td><td>0</td><td>0</td></tr></table> <div>NE</div>	0	0	0	0	12	0	0	0	0	0	0	1	0	-1	0	0	0	0	0	0	-12	0	0	0	0	<table><tr><td>-12</td><td>0</td><td>0</td><td>0</td><td>0</td></tr><tr><td>0</td><td>0</td><td>1</td><td>0</td><td>0</td></tr><tr><td>0</td><td>0</td><td>0</td><td>0</td><td>0</td></tr><tr><td>0</td><td>0</td><td>-1</td><td>0</td><td>0</td></tr><tr><td>0</td><td>0</td><td>0</td><td>0</td><td>12</td></tr></table> <div>SE</div>	-12	0	0	0	0	0	0	1	0	0	0	0	0	0	0	0	0	-1	0	0	0	0	0	0	12
0	0	12	0	0																																																																																																			
0	0	0	-1	0																																																																																																			
0	0	0	0	0																																																																																																			
0	1	0	0	0																																																																																																			
0	0	-12	0	0																																																																																																			
0	0	0	0	0																																																																																																			
0	1	0	0	0																																																																																																			
-12	0	0	0	12																																																																																																			
0	0	0	-1	0																																																																																																			
0	0	0	0	0																																																																																																			
0	0	0	0	12																																																																																																			
0	0	0	0	0																																																																																																			
0	1	0	-1	0																																																																																																			
0	0	0	0	0																																																																																																			
-12	0	0	0	0																																																																																																			
-12	0	0	0	0																																																																																																			
0	0	1	0	0																																																																																																			
0	0	0	0	0																																																																																																			
0	0	-1	0	0																																																																																																			
0	0	0	0	12																																																																																																			
<table><tr><td>0</td><td>0</td><td>-12</td><td>0</td><td>0</td></tr><tr><td>0</td><td>0</td><td>0</td><td>1</td><td>0</td></tr><tr><td>0</td><td>0</td><td>0</td><td>0</td><td>0</td></tr><tr><td>0</td><td>-1</td><td>0</td><td>0</td><td>0</td></tr><tr><td>0</td><td>0</td><td>12</td><td>0</td><td>0</td></tr></table> <div>S</div>	0	0	-12	0	0	0	0	0	1	0	0	0	0	0	0	0	-1	0	0	0	0	0	12	0	0	<table><tr><td>0</td><td>0</td><td>0</td><td>0</td><td>0</td></tr><tr><td>0</td><td>-1</td><td>0</td><td>0</td><td>0</td></tr><tr><td>12</td><td>0</td><td>0</td><td>0</td><td>-12</td></tr><tr><td>0</td><td>0</td><td>0</td><td>1</td><td>0</td></tr><tr><td>0</td><td>0</td><td>0</td><td>0</td><td>0</td></tr></table> <div>W</div>	0	0	0	0	0	0	-1	0	0	0	12	0	0	0	-12	0	0	0	1	0	0	0	0	0	0	<table><tr><td>0</td><td>0</td><td>0</td><td>0</td><td>-12</td></tr><tr><td>0</td><td>0</td><td>0</td><td>0</td><td>0</td></tr><tr><td>0</td><td>-1</td><td>0</td><td>1</td><td>0</td></tr><tr><td>0</td><td>0</td><td>0</td><td>0</td><td>0</td></tr><tr><td>12</td><td>0</td><td>0</td><td>0</td><td>0</td></tr></table> <div>SW</div>	0	0	0	0	-12	0	0	0	0	0	0	-1	0	1	0	0	0	0	0	0	12	0	0	0	0	<table><tr><td>12</td><td>0</td><td>0</td><td>0</td><td>0</td></tr><tr><td>0</td><td>0</td><td>-1</td><td>0</td><td>0</td></tr><tr><td>0</td><td>0</td><td>0</td><td>0</td><td>0</td></tr><tr><td>0</td><td>0</td><td>1</td><td>0</td><td>0</td></tr><tr><td>0</td><td>0</td><td>0</td><td>0</td><td>-12</td></tr></table> <div>NW</div>	12	0	0	0	0	0	0	-1	0	0	0	0	0	0	0	0	0	1	0	0	0	0	0	0	-12
0	0	-12	0	0																																																																																																			
0	0	0	1	0																																																																																																			
0	0	0	0	0																																																																																																			
0	-1	0	0	0																																																																																																			
0	0	12	0	0																																																																																																			
0	0	0	0	0																																																																																																			
0	-1	0	0	0																																																																																																			
12	0	0	0	-12																																																																																																			
0	0	0	1	0																																																																																																			
0	0	0	0	0																																																																																																			
0	0	0	0	-12																																																																																																			
0	0	0	0	0																																																																																																			
0	-1	0	1	0																																																																																																			
0	0	0	0	0																																																																																																			
12	0	0	0	0																																																																																																			
12	0	0	0	0																																																																																																			
0	0	-1	0	0																																																																																																			
0	0	0	0	0																																																																																																			
0	0	1	0	0																																																																																																			
0	0	0	0	-12																																																																																																			

**Legend:** *N* = North, *S* = South, *E* = East, *W* = West,  
*NE* = Northeast, *NW* = Northwest, *SE* = Southeast

Figure 3.6: Directional 5 x 5 magic square operators.

### 3.4 Magic Cube

The magic cube is a 3-D extension of the magic square. A magic cube of order  $N$  is composed of entries  $1, 2, \dots, N^3$  or  $0, 1, \dots, N^3 - 1$  arranged in a cubic lattice such that the sum of all entries along the rows, columns, pillars and four main space diagonals are equal to a magic constant (Andrews, 2004). The magic constant can be found as

$$C = \frac{N}{2}(N^3 + 1) \quad (3.3)$$

for elements ranging from  $1, 2, \dots, N^3$  and

$$C = \frac{N}{2}(N^3 - 1) \quad (3.4)$$

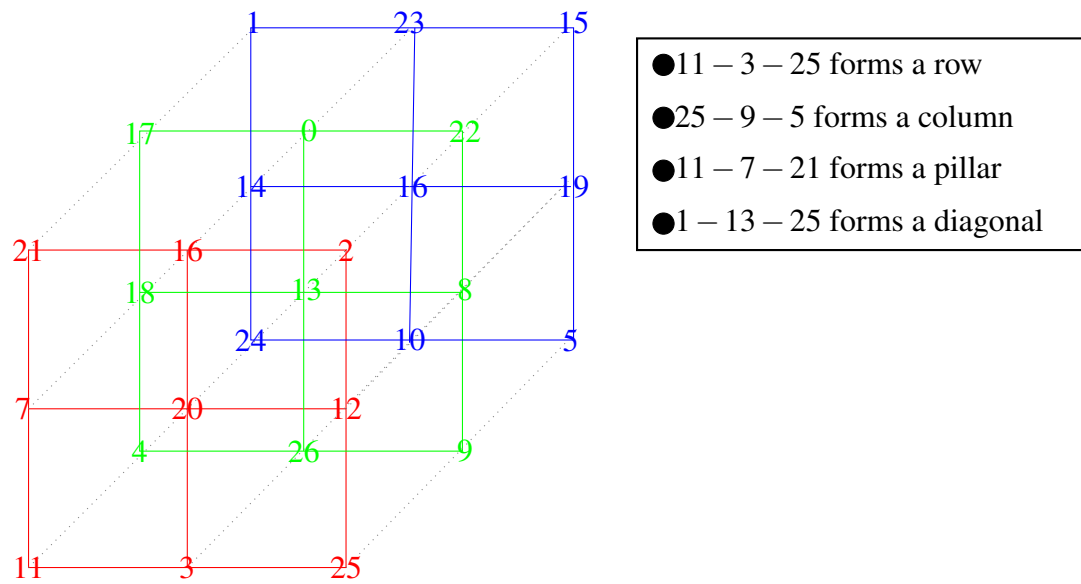
for elements ranging from  $0, 1, \dots, N^3 - 1$

A magic cube has four basic distinct forms that are not covered here in this work. Each of these four has 48 aspects formed by rotation and/or reflection making a total of 192 aspects (Heinz and Hendricks, 2000). Figure 3.7 shows one aspect of the  $3 \times 3 \times 3$  normal magic cube formed by integers  $0 - 26$  with a magic constant of 39.

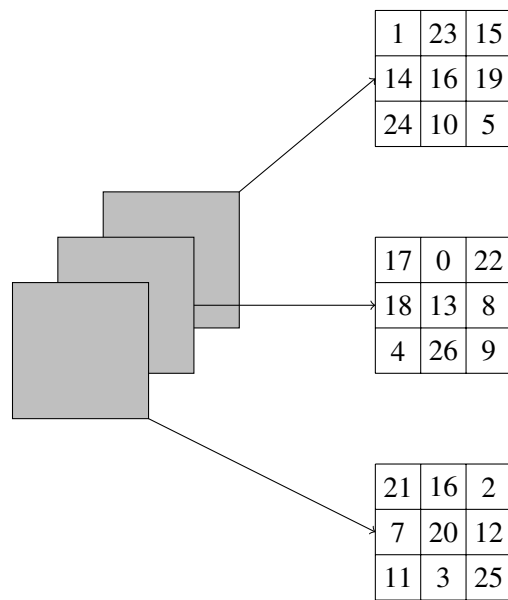
Based on the concept of magic square operator by Chen and Nie (2007), Al-Shuhail and Al-Dossary (2014) constructed 3-D kernels of the magic cube operator from the  $3 \times 3 \times 3$  normal magic cube and used them to find the direction along which amplitude change is maximum. They found that there are only seven distinct directions along

which the absolute difference across the central element is maximum. Their procedure is as follows:

- i Start with the seven magic cube aspects that have the maximum absolute difference across the center element (Figure 3.8).
- ii Subtract the central element from all elements of these magic cubes to produce the corresponding seven templates.
- iii Zero all elements of these templates except the absolute maxima and minima to produce the corresponding seven kernels (Figure 3.9):  $K_i (i = 1, 2, \dots, 7)$
- iv Perform 3-D convolution (Tertois and Frank, 2004) of the resulting seven masks (i.e., kernels) with the 3 x 3 x 3 cube centered on the point of interest in the input 3-D seismic data (D). This produces seven gradient magnitudes:  $D * K_i$
- v The maximum convolution value is selected as the edge (E) at the point of interest and its mask defines the edge direction:  $E = \max_{i=1}^7 (D * K_i)$



(a)



(b)

Figure 3.7: Normal magic cube operators.

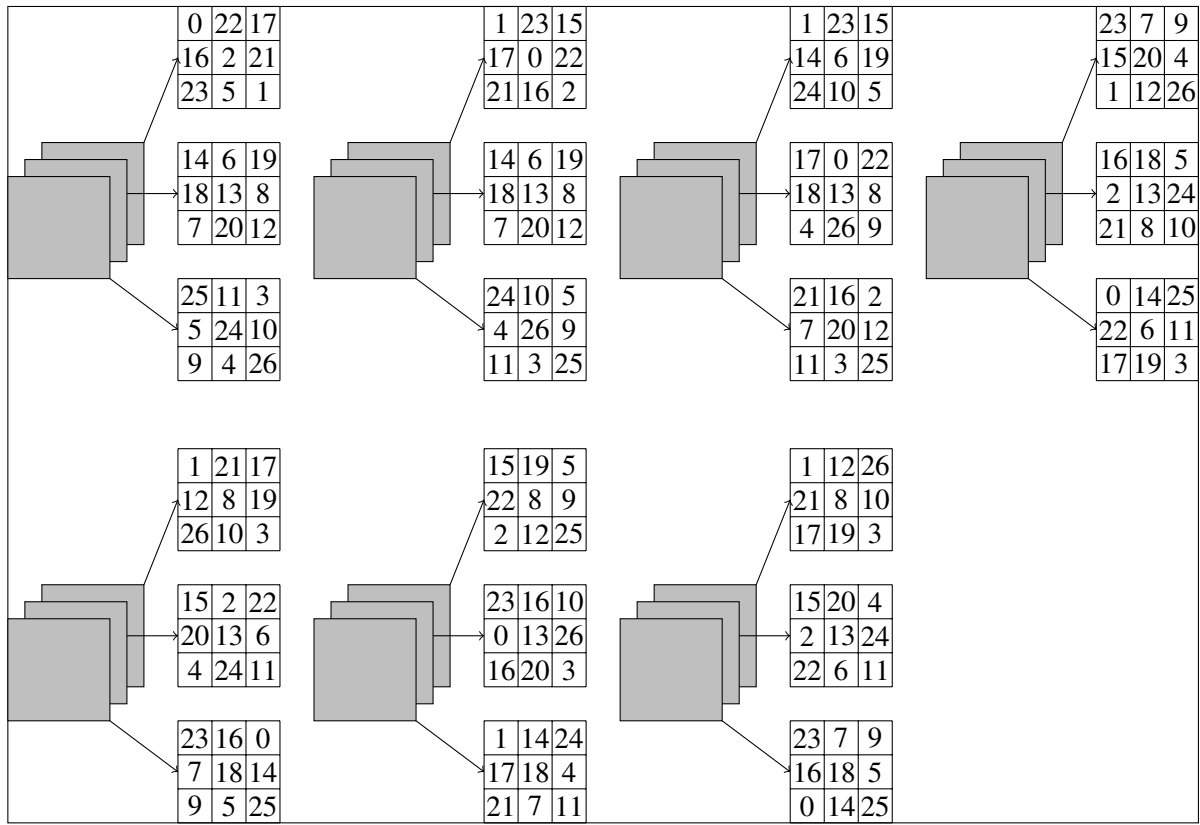


Figure 3.8: Seven magic cube kernels (after Al-Shuhail and Al-Dossary, 2014).

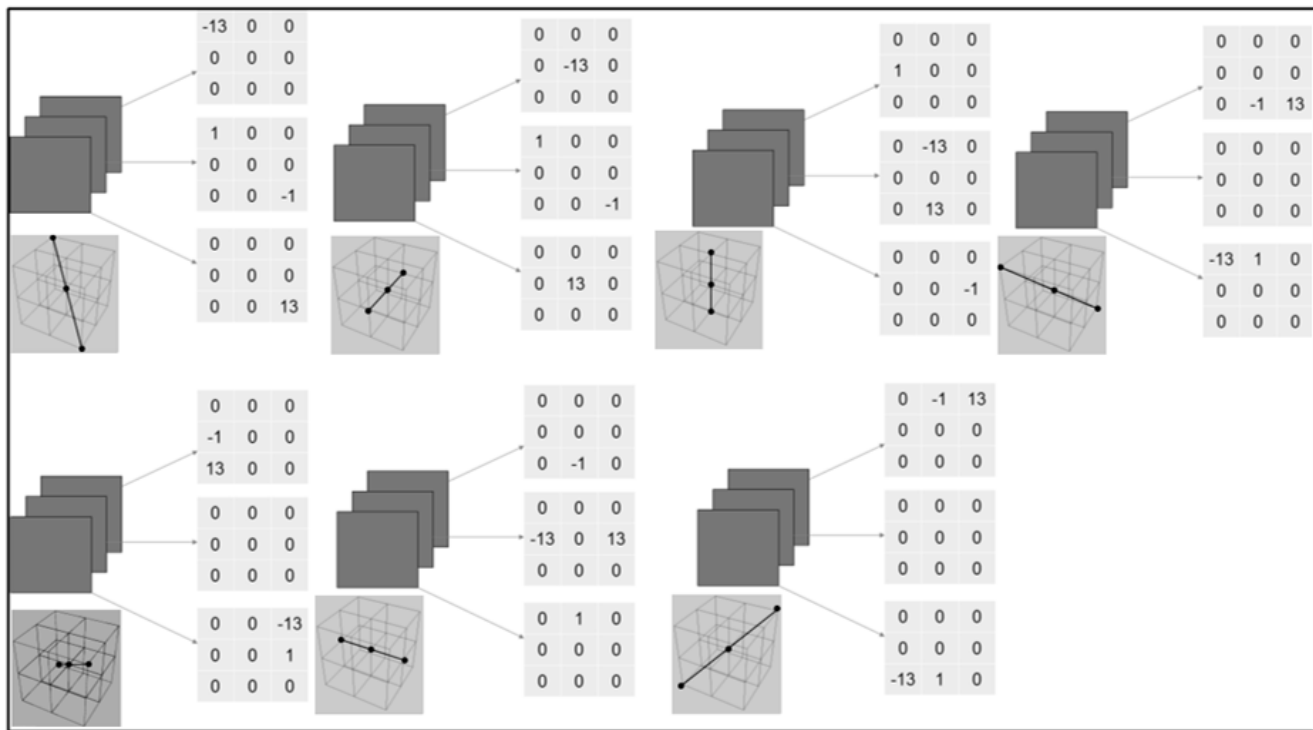


Figure 3.9: The corresponding edge detection kernels along with their associated directions of maximum gradient in 3-D space (after Al-Shuhail and Al-Dossary, 2014).

### 3.5 Modified $F_2$ Magic cube Operator

Al-Shuhail and Al-Dossary (2014) extended the magic square to magic cube, an approximate differential operator, based on the implementation procedure for the magic square by Chen and Nie (2007) with seven magic cubes as initial matrices.

In an attempt to produce good result especially when searching for channels in time slices, I apply their procedure on seismic data in this section. Based on the results obtained from the magic cube operator by Al-Shuhail and Al-Dossary (2014), I used the magic cube in which the maximum element lies in the second vertical slice. Such an arrangement becomes a choice for the initial matrix of the modified algorithm. My procedure is shown in Figure 3.10, while Figures 3.11-3.13 show application of the procedure to the normal  $3 \times 3 \times 3$  magic cube.

The  $3 \times 3 \times 3$  magic cube is also extended to  $5 \times 5 \times 5$  (see Figure 3.16) following the same procedures. The initial matrix found to have this property is that of Andrews (2004), although  $5 \times 5 \times 5$  magic cube by Trump and Boyer (Boyer, 2003) can be permuted to have this form (Figures 3.14-3.15). They comprise elements 1 – 125 with central element 63 and magic constant of 315. They both belong to perfect magic cube since all rows, columns, diagonals and space diagonals sum to magic constant. The corresponding directions scanned by kernels, K-5a, K-6a, K-7a, K-8a and their  $5 \times 5 \times 5$  equivalents are illustrated in Figure 3.17



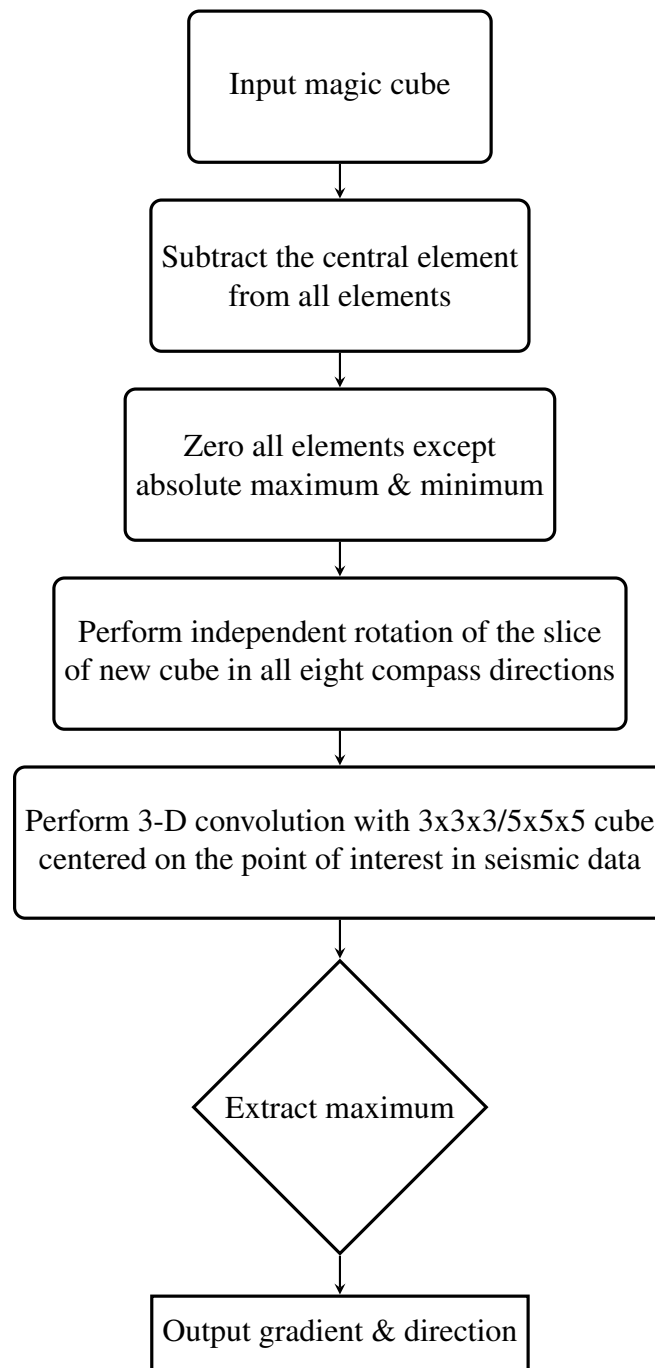


Figure 3.10: Flowchart of the procedure to construct and apply the proposed magic cube operator.

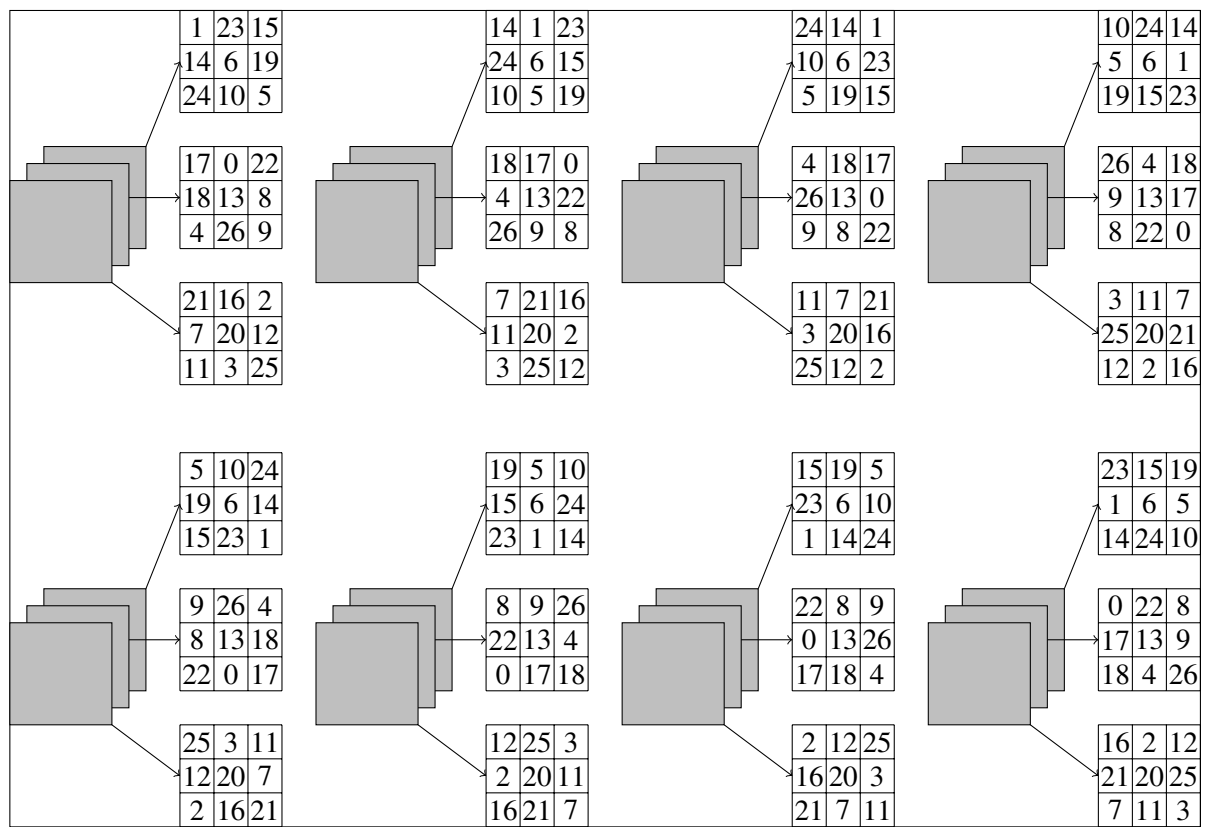


Figure 3.11: Eight magic cubes produced by the modified algorithm.

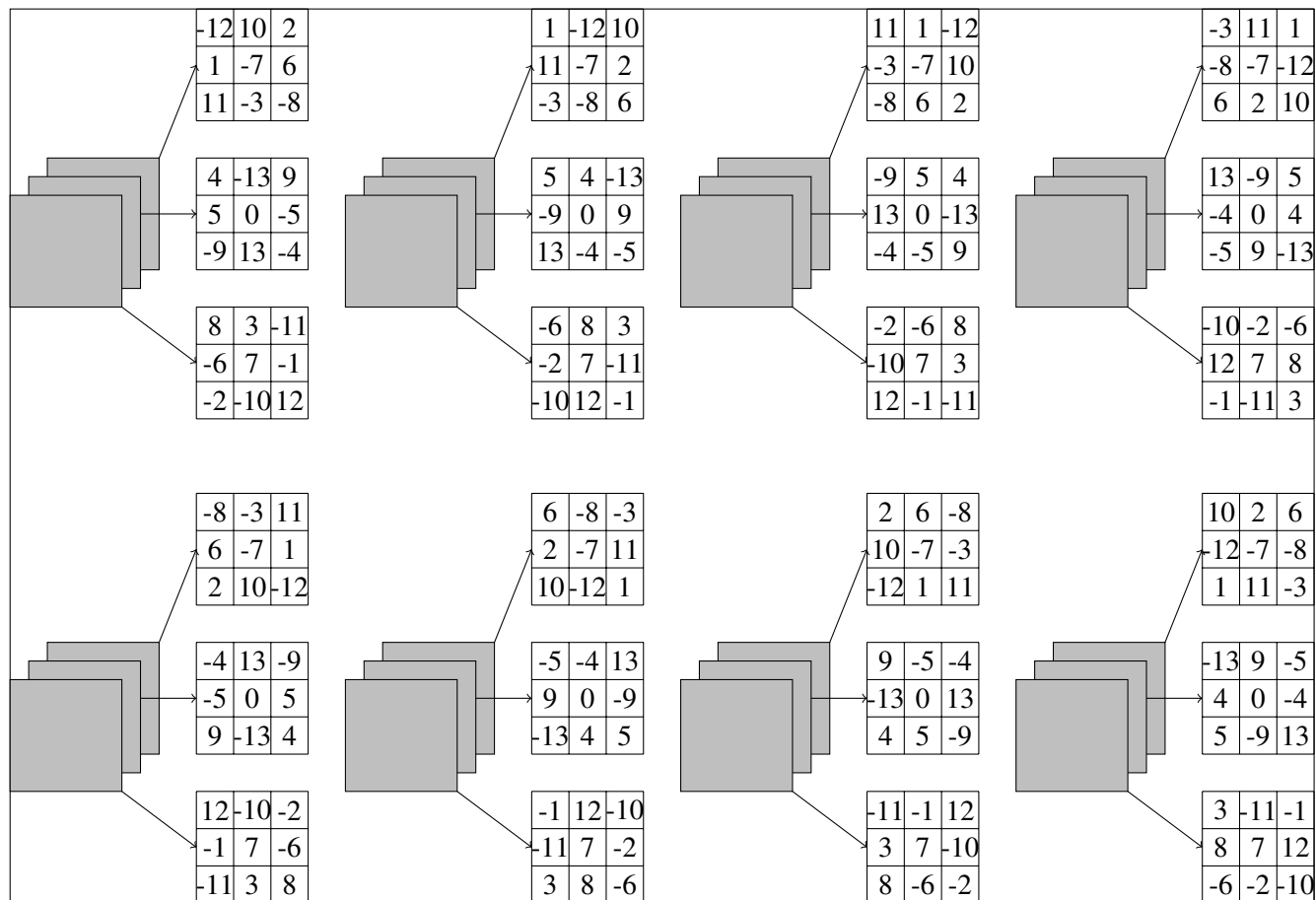


Figure 3.12: Templates derived from the eight magic cubes.

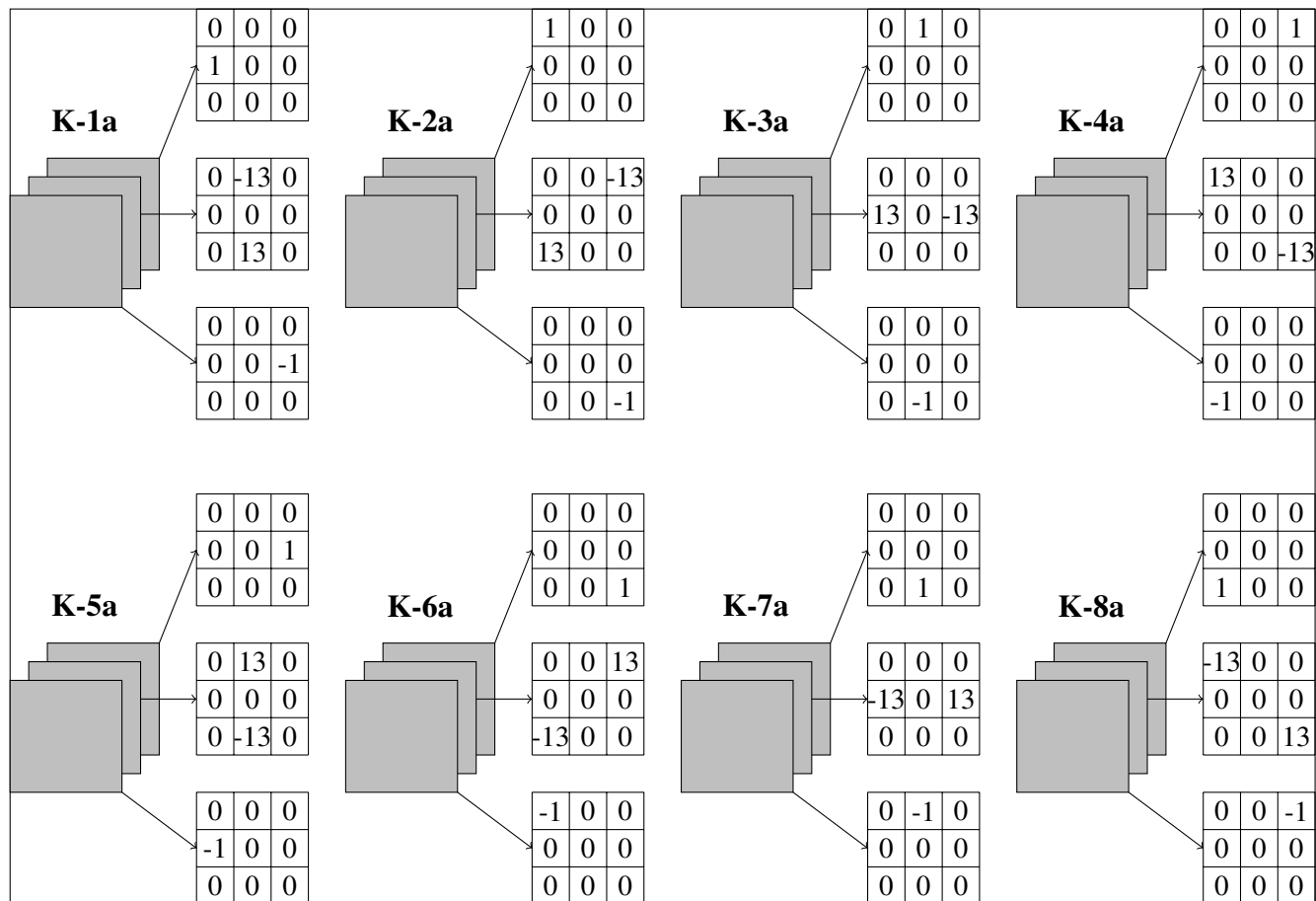
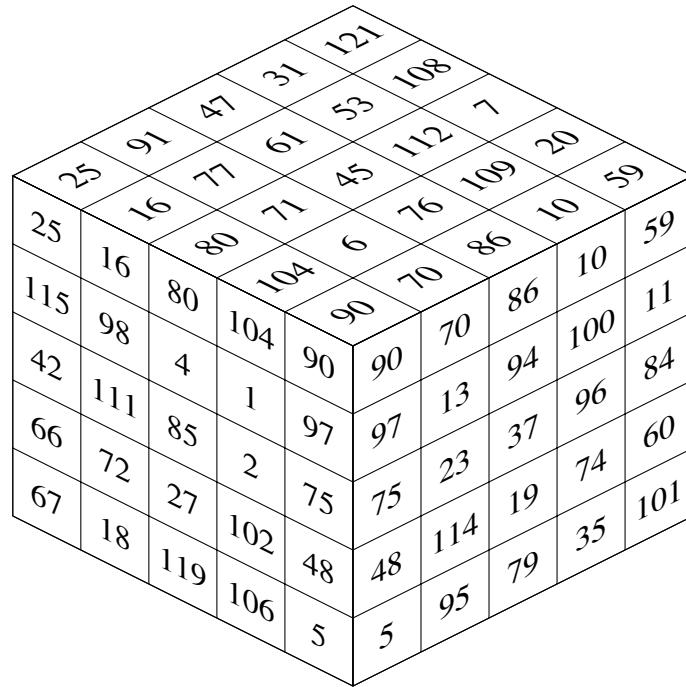
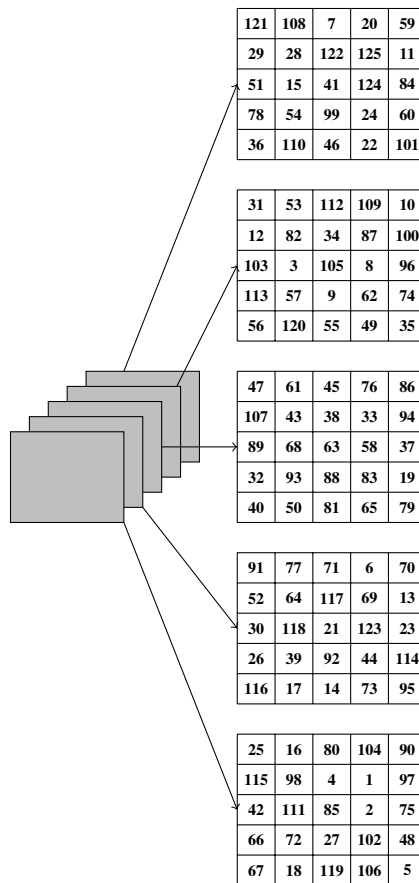


Figure 3.13: The corresponding 3 x 3 x 3 edge detection kernels.

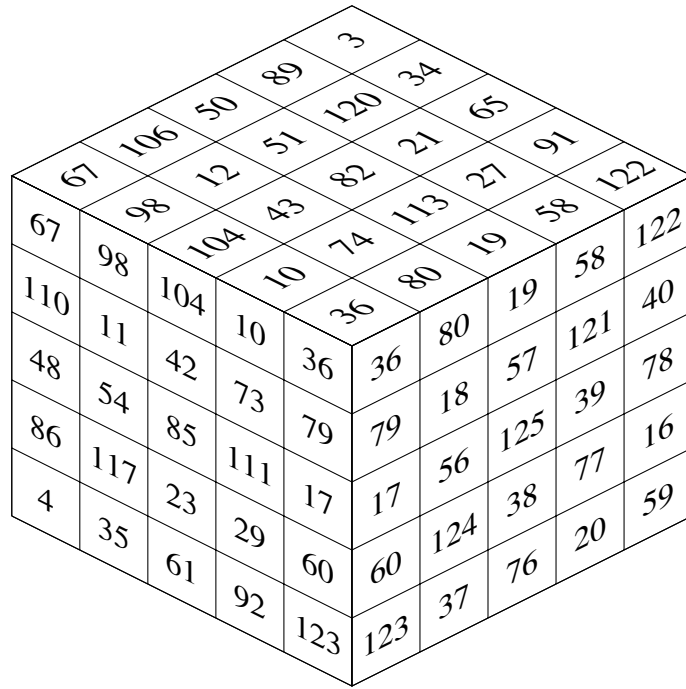


(a)

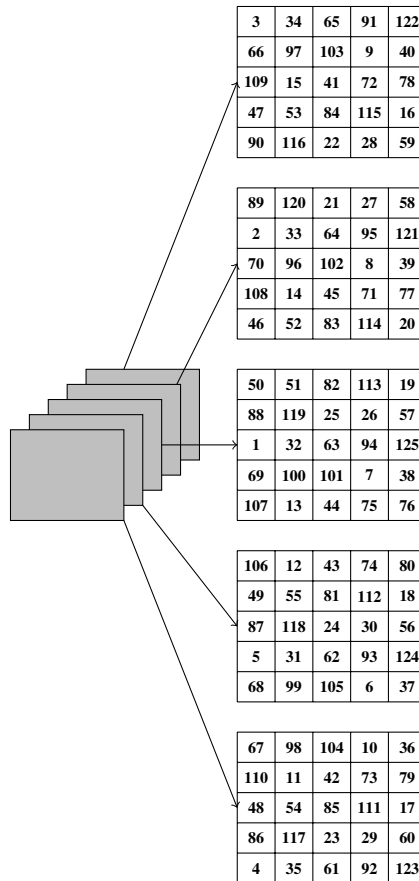


(b)

Figure 3.14: Normal magic cube by Trump and Boyer (Boyer, 2003).

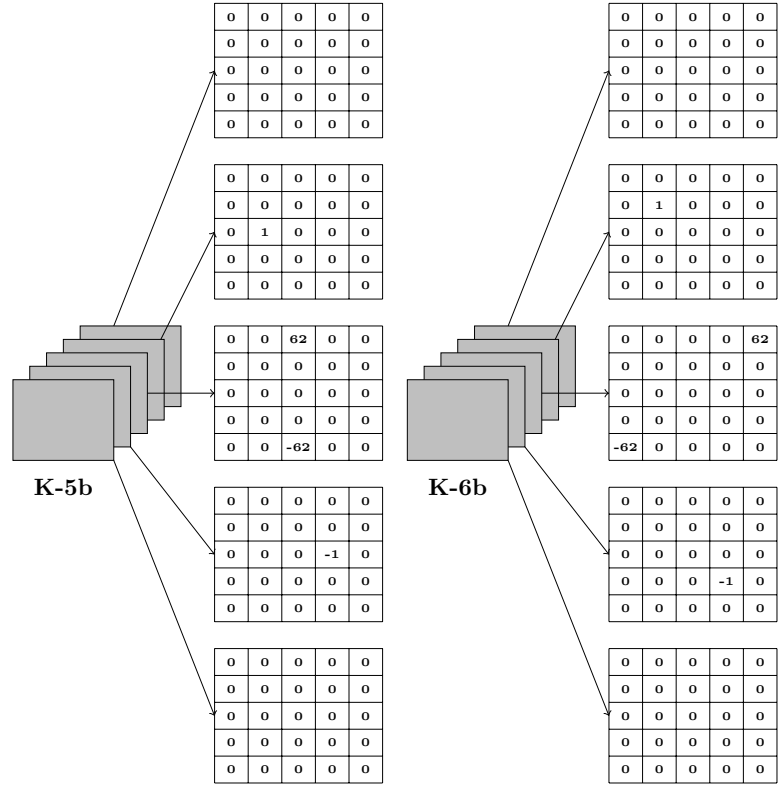


(a)



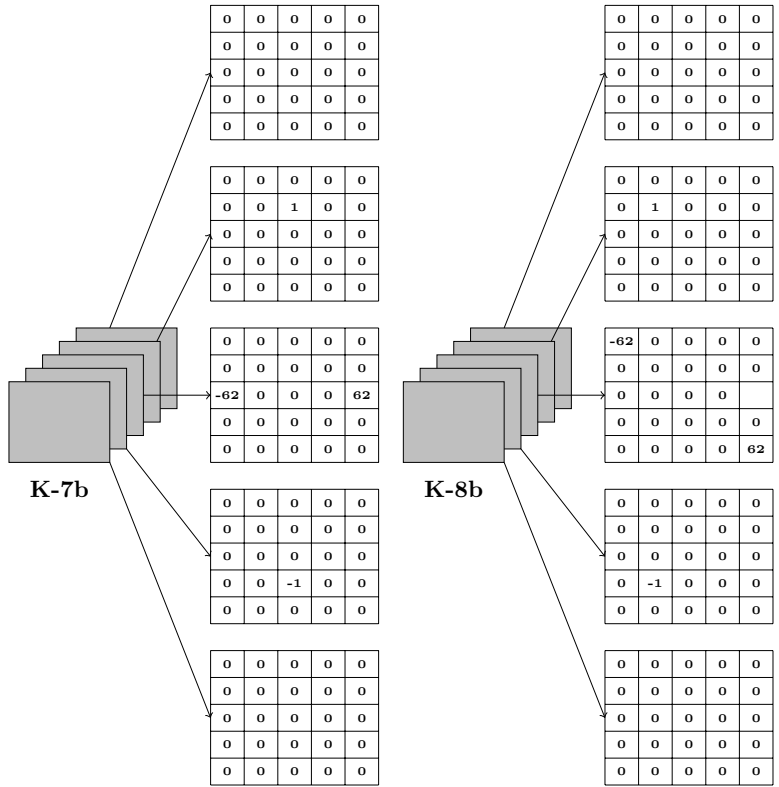
(b)

Figure 3.15: Normal magic cube (Andrews, 2004).



(a)

(b)



(c)

(d)

Figure 3.16: The corresponding 5 x 5 x 5 edge detection kernels.

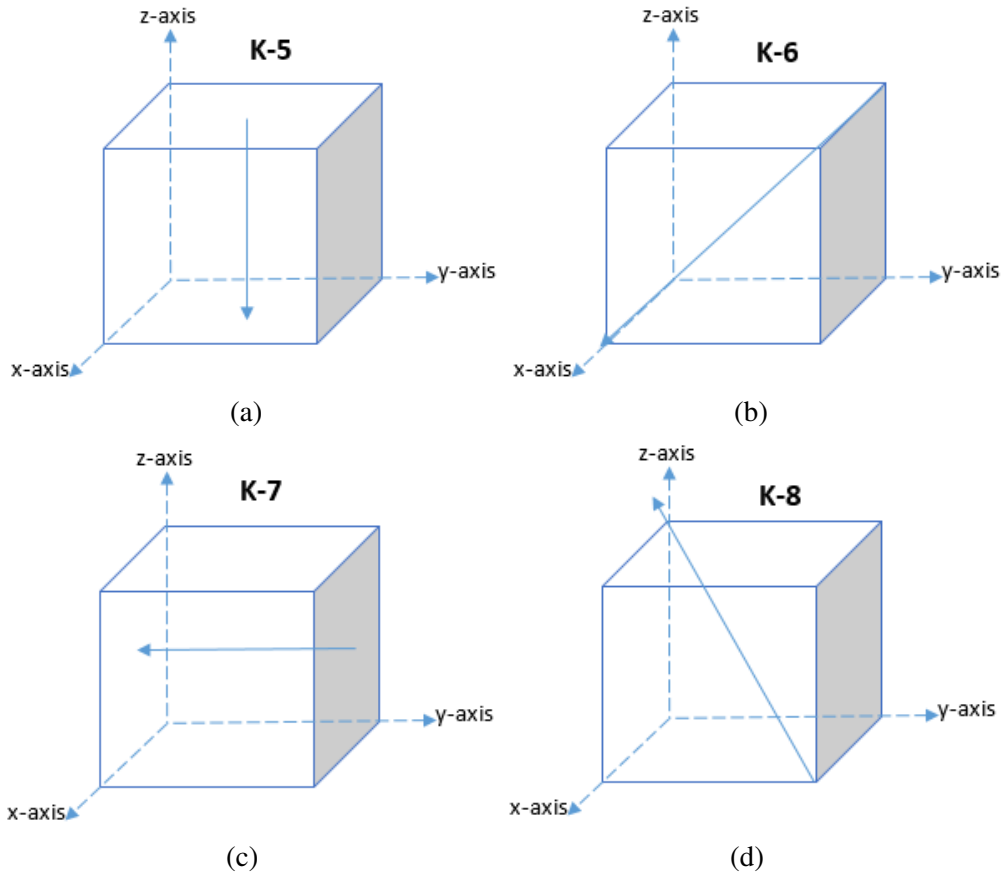


Figure 3.17: Schematic illustration of directions scanned by the kernels (shown by the solid arrow).



# **CHAPTER 4**

## **APPLICATION**

### **4.1 Data Summary**

In order to test the performance of the proposed two methods, experiments were implemented using a real 3-D seismic data provided by Saudi Aramco. The data is sampled at 4 ms and consists of 630 inlines, 560 crosslines and 300 time slices. The data (Figures 4.1-4.2) is appropriate for this study because it contains interesting geologic features such as a channel system and a continuous horizon of weak/moderate amplitude. Other information such as depositional environment, tectonic history and general geology of the area were not provided due to proprietary reason.

### **4.2 Examples**

In this section, the edge detection capability of magic square and cube operators is demonstrated using a data volume and a time slice. The performance of the operator is compared with that of Sobel (3-D Sobel is shown in the Appendix).

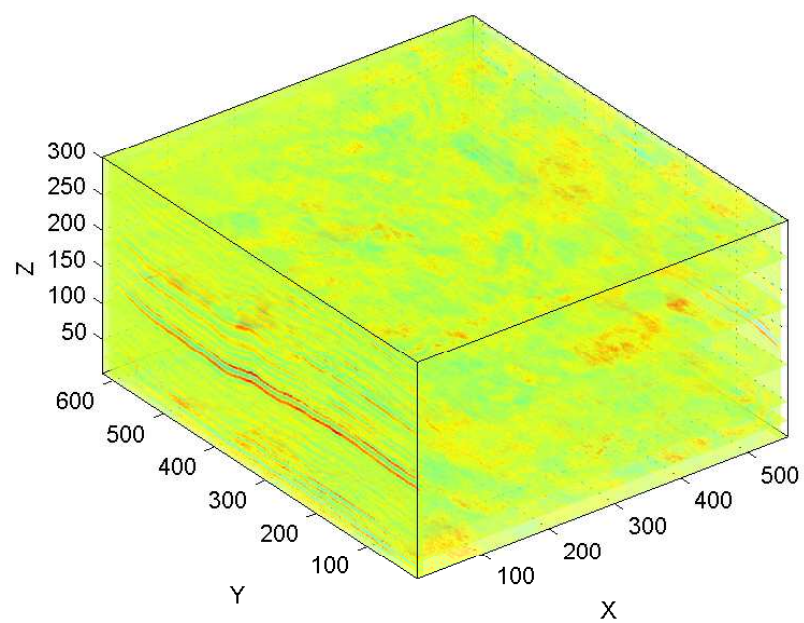


Figure 4.1: 3-D seismic volume. (X = Crossline, Y = Inline, Z = Time slice)

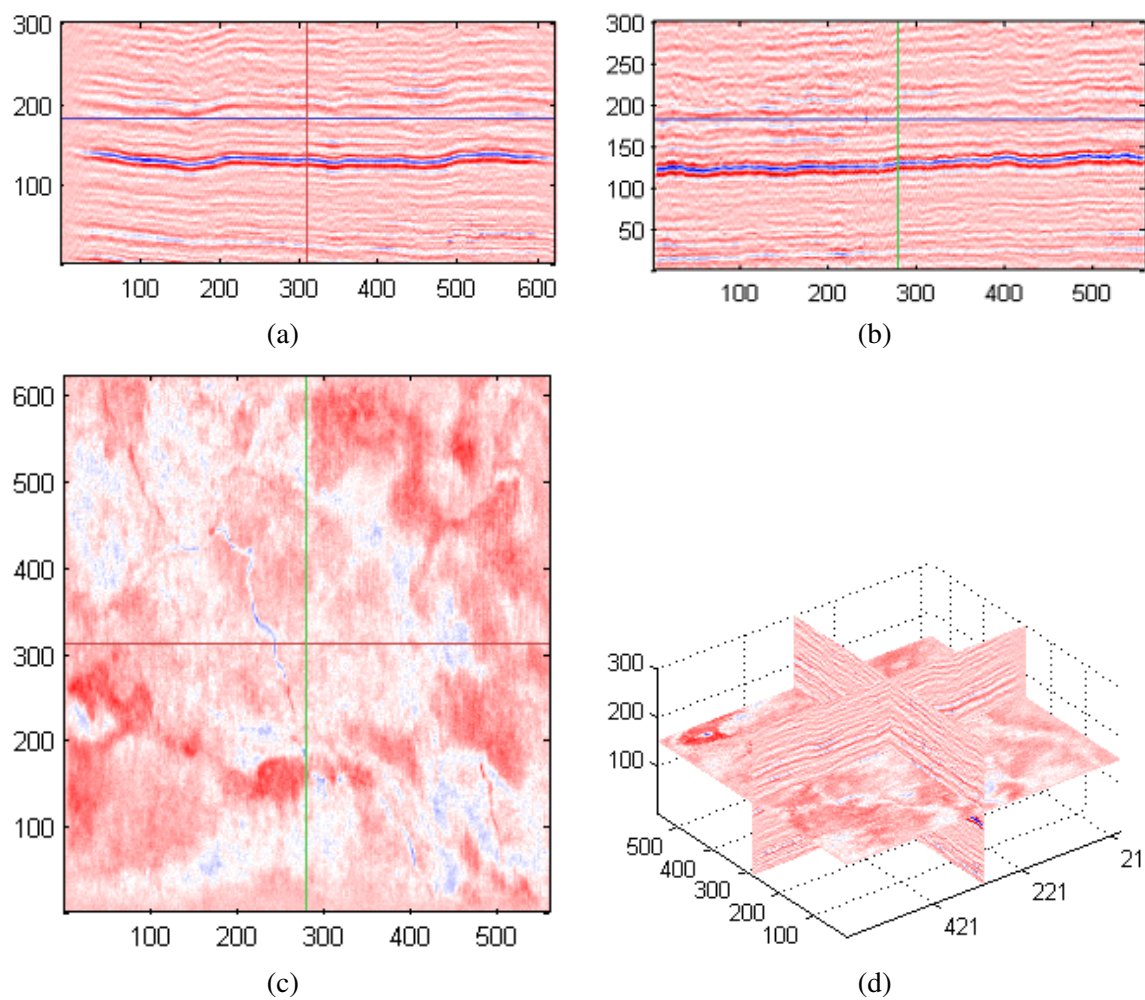


Figure 4.2: Extracted slices from the 3-D seismic volume; (a) Inline 280, (b) Crossline 310, (c) Time slice extracted at 720 ms and (d) 3-D display of these slices.

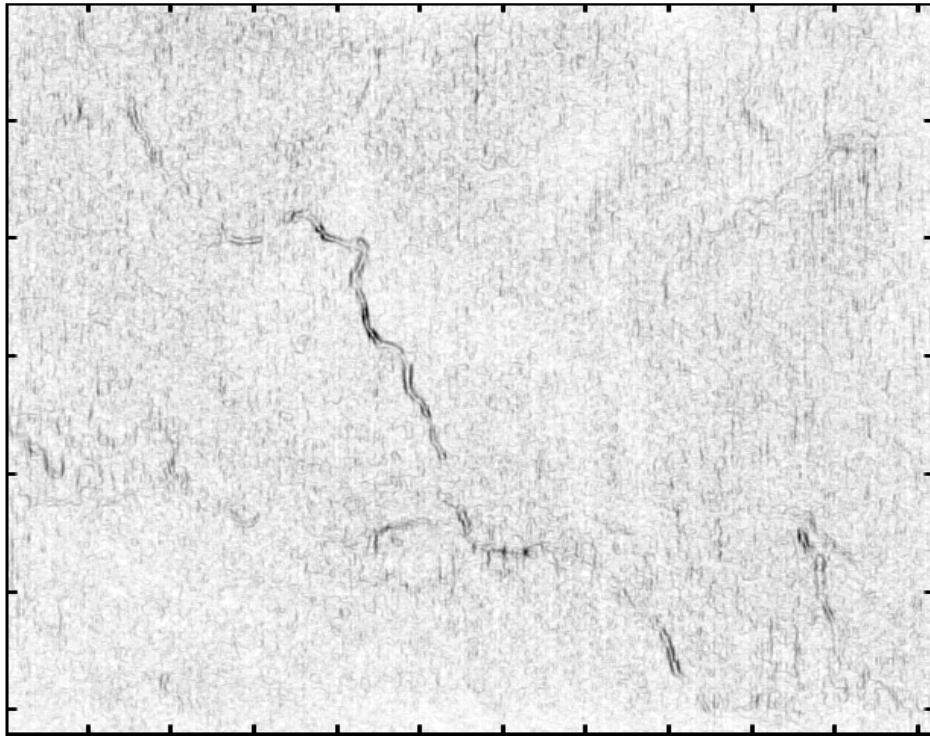
### 4.2.1 Magic Square Example

The example for the 2-D case utilizes a time slice at 720 ms from the seismic volume. Figure 4.2c shows the extracted time slice which serves as input data into the magic square algorithms. The time slice consists of meandering channels trending SE-NW in the presence of background geology. Figure 4.3 presents the result of 3 x 3 magic square  $F_1$  operator, while Figure 4.4 presents the results of magic square  $F_2$  operator which also shows the amplitude gradient magnitude and their respective orientations. Figure 4.6 shows corresponding maps for 5 x 5 magic square  $F_2$  operator. These figures show the good performance of the magic square operator in delineating geological features trending perpendicular to the operator direction. Figures 4.5 and 4.7 show the result of the maximum convolution values collected over all four compass directions. This result combines all the geologic features in each of the kernels leading to high resolution and enhanced output.

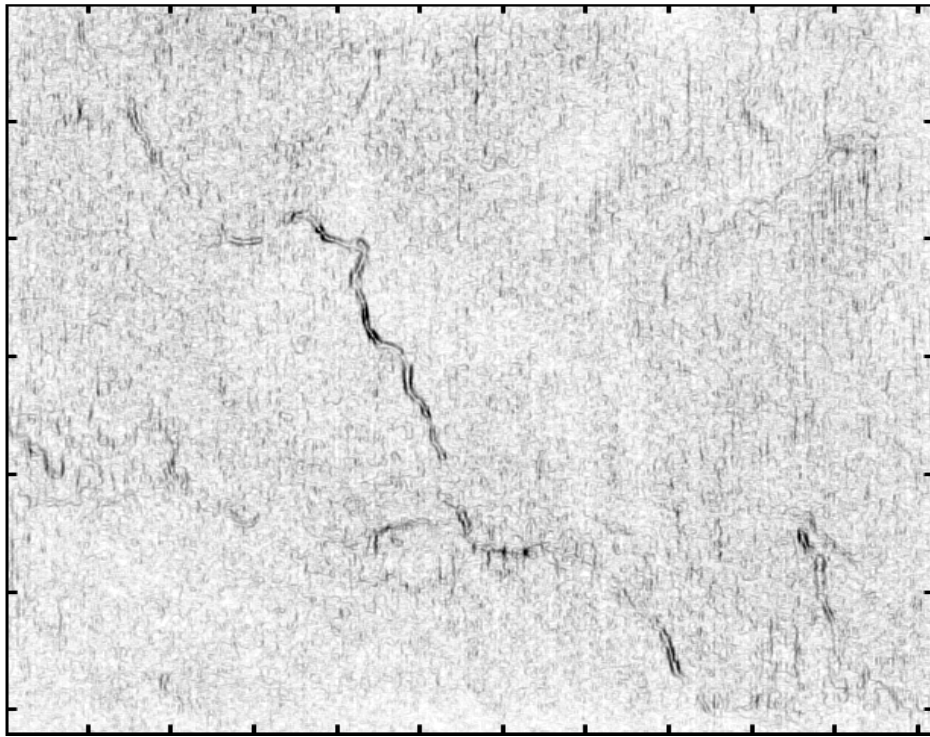
Figures 4.8a and 4.8b compare the 3 x 3 Sobel operator to 3 x 3 magic square  $F_1$  operator, while Figures 4.8c and 4.8d compare the 5 x 5 Sobel to 5 x 5 magic square  $F_1$  operator. Figures 4.9a and 4.9b compare the 3 x 3 Sobel operator to 3 x 3 magic square  $F_2$  operator, while Figures 4.9c and 4.9d compare the 5 x 5 Sobel to 5 x 5 magic square  $F_2$  operator. In all of these comparison, it is clear that the results of the magic square and 2-D Sobel operators are generally comparable.

For further comparison, I investigated the efficiency and robustness of the operators

in the presence of noise. A random Gaussian noise of zero mean and 0.1 standard deviation was added to the data (Figure 4.10) and the corresponding outputs of the operators are presented in Figure 4.11. The channels (indicated by the blue and green arrows) are completely masked in the output of the 3 x 3 magic square  $F_2$  operator.



(a)



(b)

Figure 4.3: Gradient edge maps of the 3 x 3 magic square  $F_1$  with (a)  $M_1$  and (b)  $M_3$ .

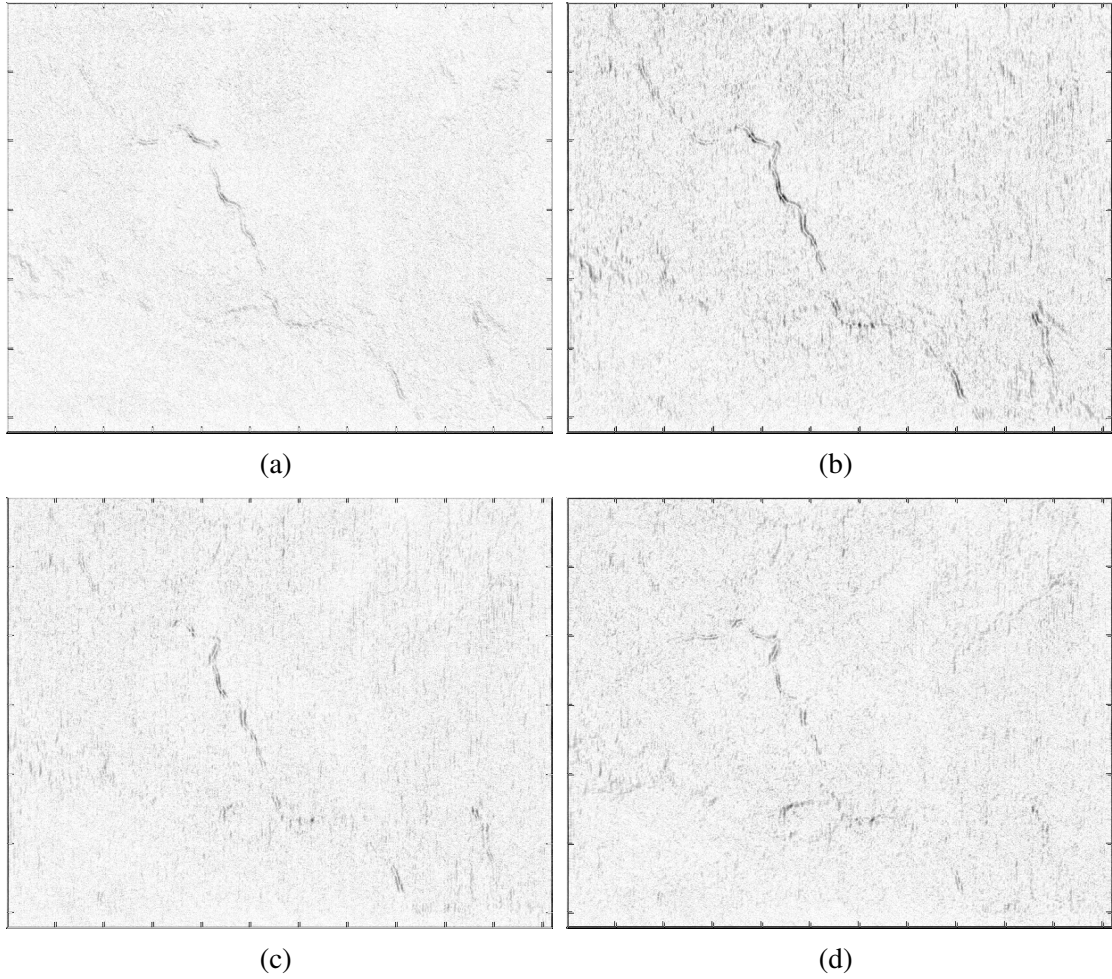


Figure 4.4: Gradient edge maps of the  $3 \times 3$  magic square  $F_2$  operator along (a) North direction, (b) Northeast direction, (c) East direction and (d) Southeast direction.

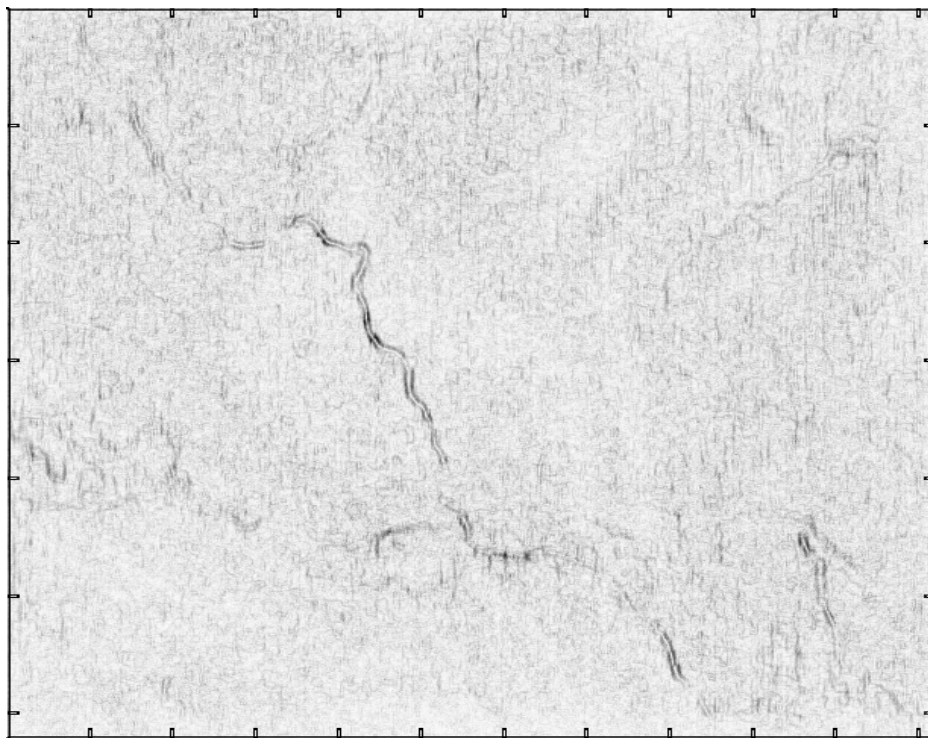


Figure 4.5: Maximum gradient edge map of the 3 x 3 magic square  $F_2$  operator.



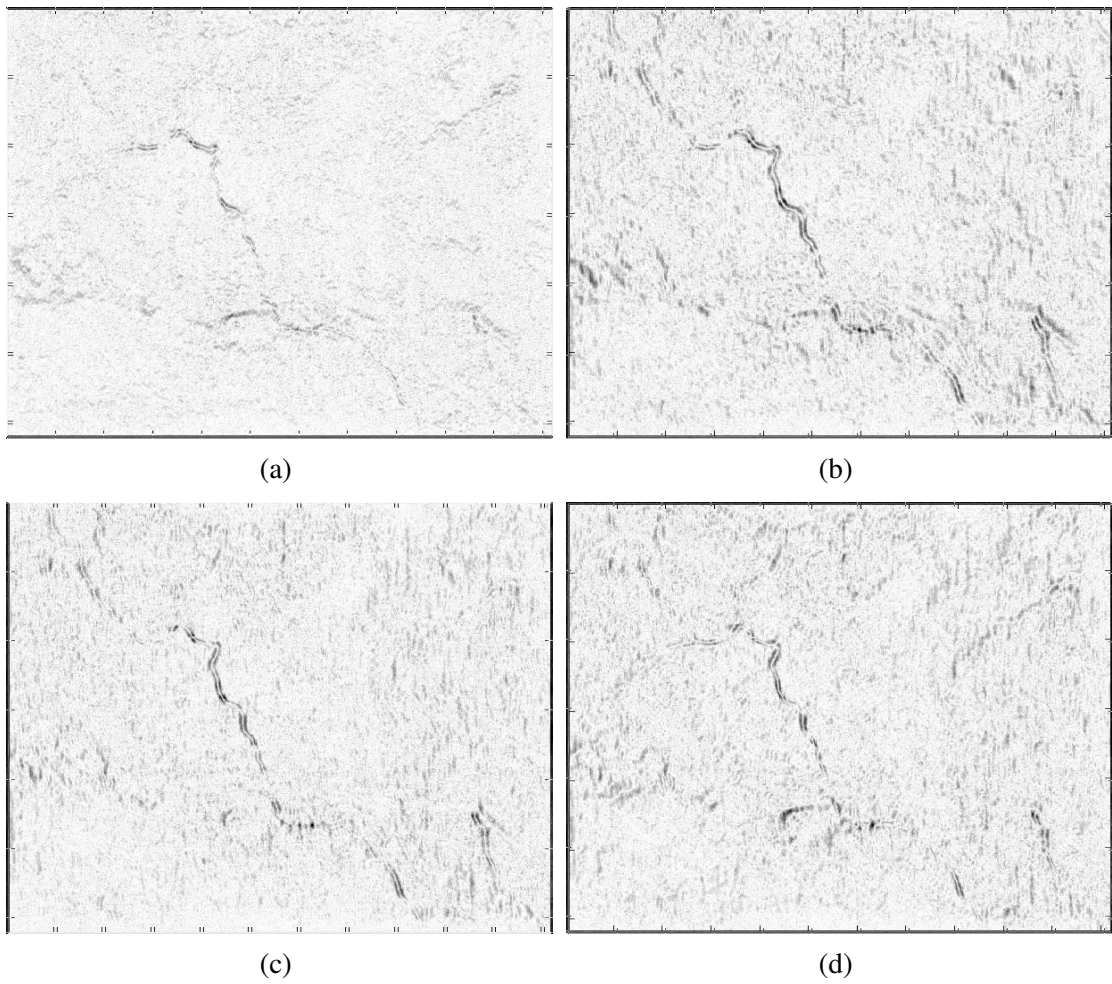


Figure 4.6: Gradient edge maps of the 5 x 5 magic square  $F_2$  operator along (a) North direction, (b) Northeast direction, (c) East direction and (d) Southeast direction.

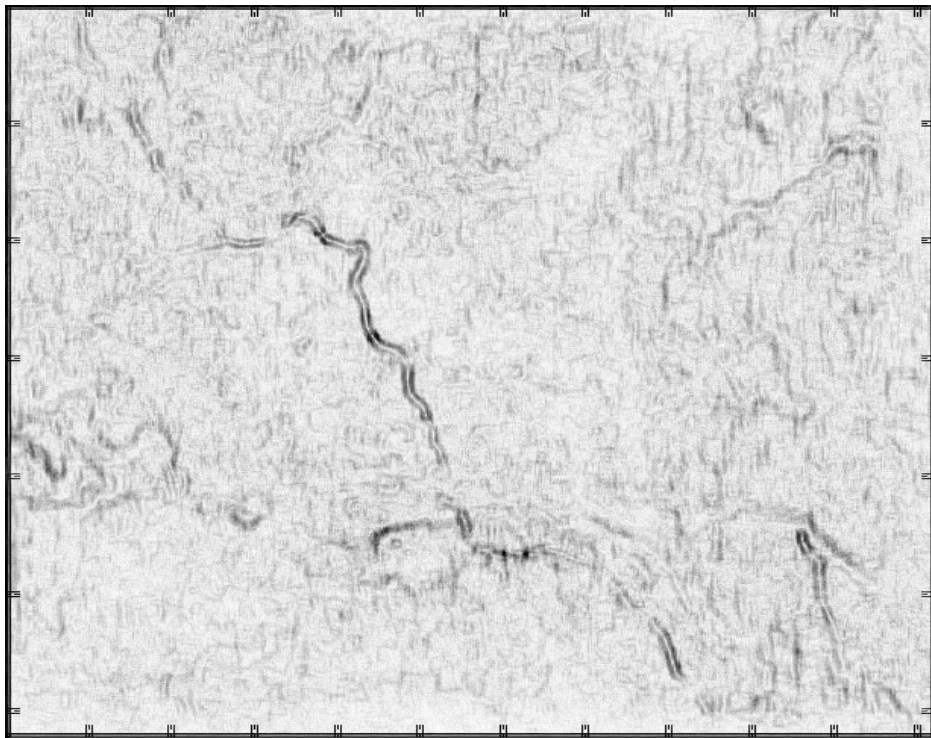


Figure 4.7: Maximum gradient edge map of the 5 x 5 magic square  $F_2$  operator.

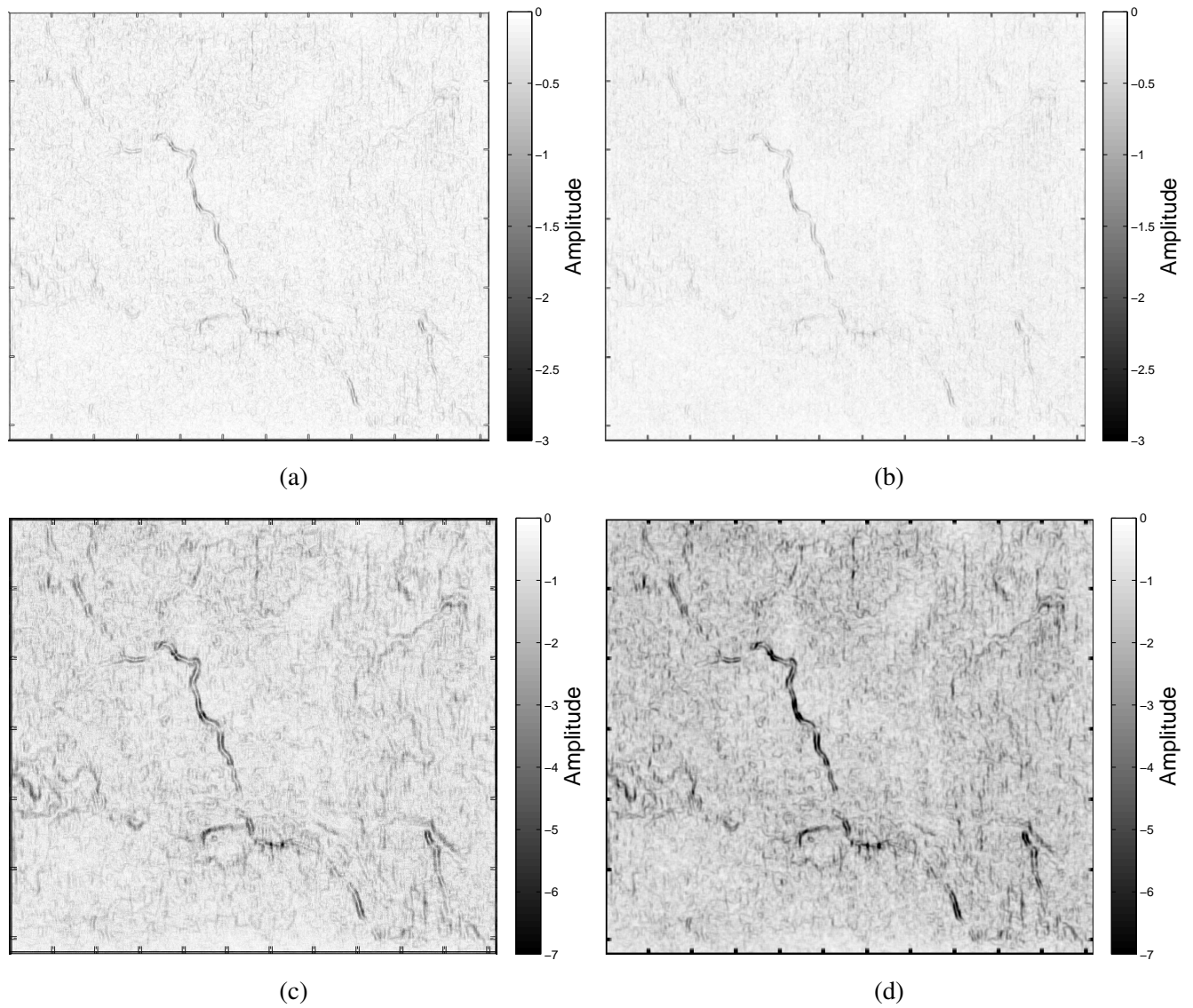


Figure 4.8: Comparison of gradient edge maps; (a) 3 x 3 Sobel operator, (b) 3 x 3 magic square  $F_1$  operator; (c) 5 x 5 Sobel operator and (d) 5 x 5 magic square  $F_1$  operator.

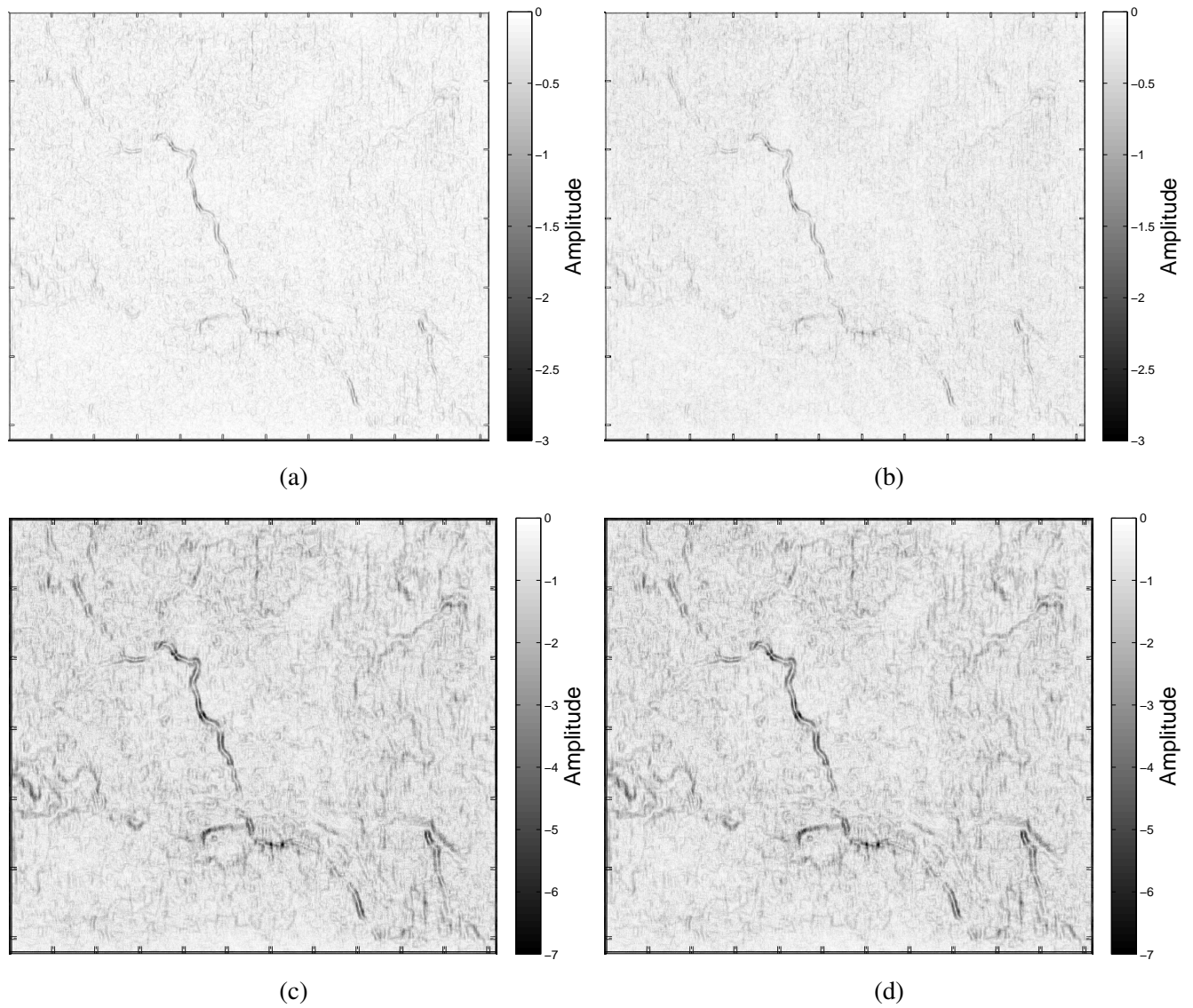


Figure 4.9: Comparison of gradient edge maps; (a) 3 x 3 Sobel operator, (b) 3 x 3 magic square  $F_2$  operator, (c) 5 x 5 Sobel operator and (d) 5 x 5 magic square  $F_2$  operator.

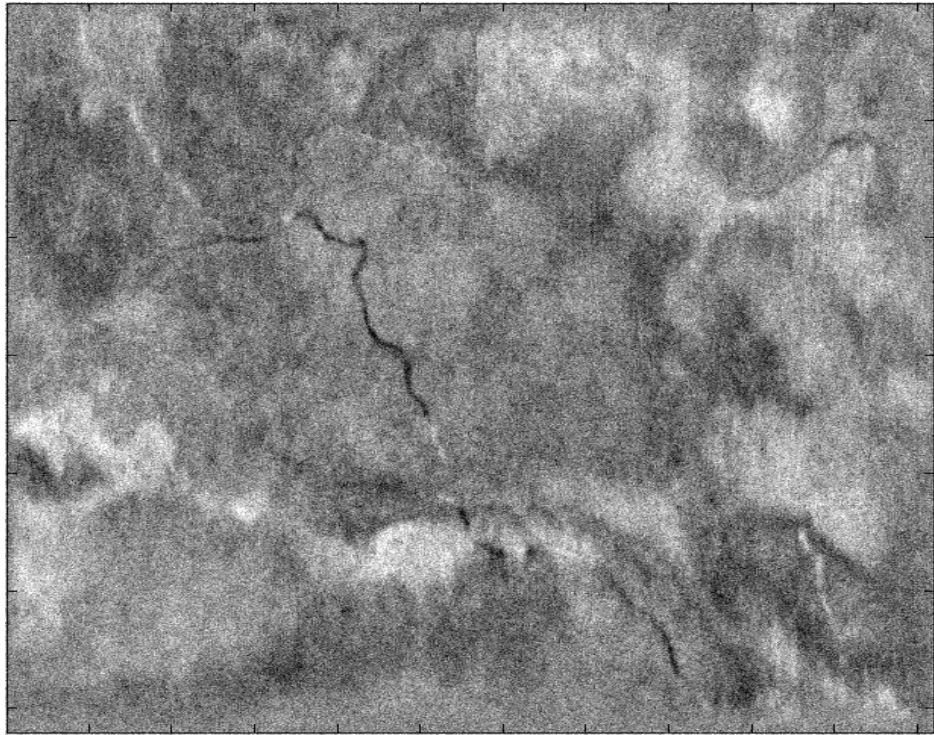
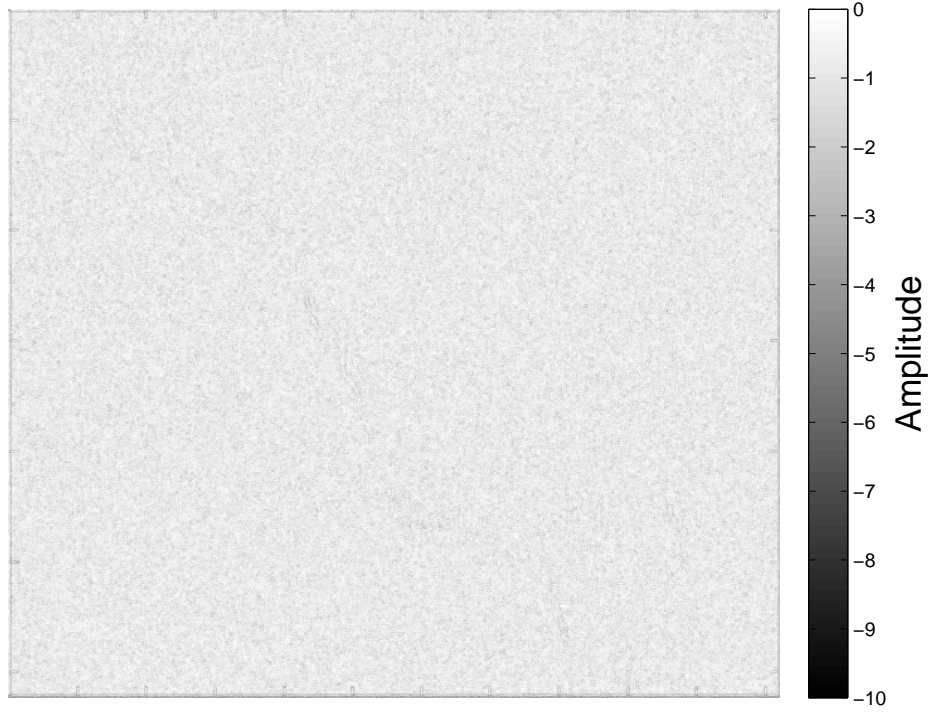
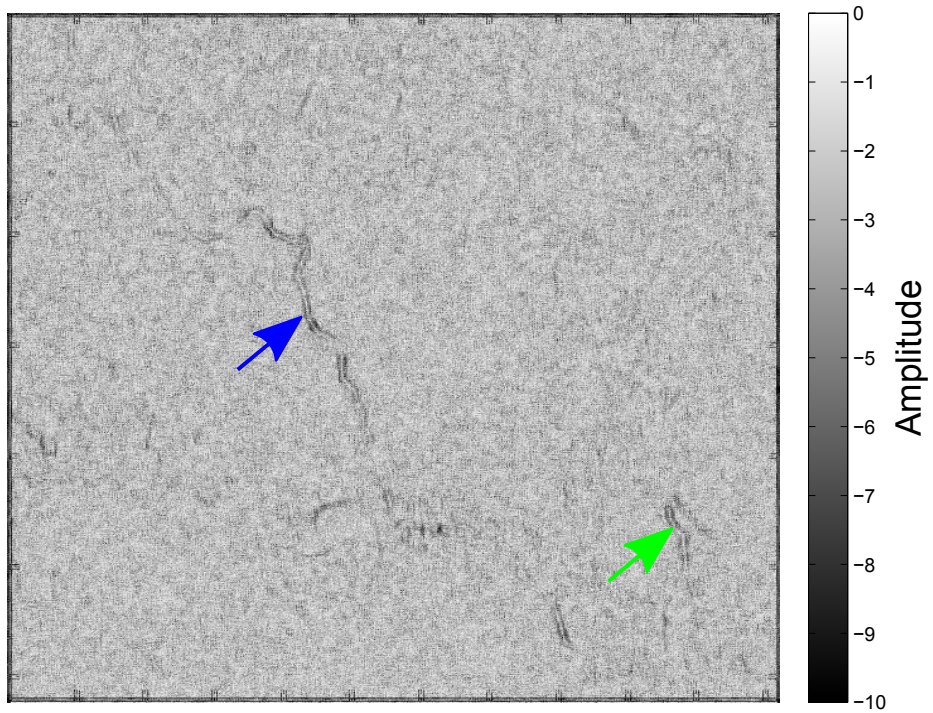


Figure 4.10: Time slice with Gaussian noise of zero mean and 0.1 standard deviation.





(a)



(b)

Figure 4.11: Comparison of gradient edge maps in the presence of noise using (a) 3 x 3 magic square  $F_2$  kernel and (b) 5 x 5 magic square  $F_2$  kernel. The delineation of the two channels (blue and green arrows) suggests that the higher spatial dimension is better for data with noise.

### 4.2.2 Magic Cube Example

The example for the 3-D case utilizes the seismic volume. Results of the  $3 \times 3 \times 3$  magic cubes are presented in Figure 4.12. The results demonstrate the multidirectional characteristics of the kernels. For example, K-5a performs poorly in delineating the channel system because it scans in north-south orientation and hence is only capable of effectively delineating EW trending seismic features. The K-6a clearly and effectively delineates the channels since the kernel runs perpendicularly to the geological feature. Figure 4.13 shows inline 5 and its gradient edge map.

Figure 4.14 presents the results of implementing the  $5 \times 5 \times 5$  magic cube operators. The results are better compared with that of smaller spatial window. The amplitude gradient map of inline 5 (Figure 4.15b) gives a good definition of events. The events at the lower and upper parts of the map are clearly enhanced. Figures 4.16-4.17 presents the comparison between time slice and inline amplitude gradient maps obtained by implementing the  $3 \times 3 \times 3$  and  $5 \times 5 \times 5$  magic cubes versus Sobel operator respectively. The results are normalized properly to allow for fair comparison. In general, the result of the magic cube operator with the larger spatial window produces better definition of the channel system. The Sobel delineates the channel system but not without some background noise. The results of inline gradient map is better in magic cubes than in the Sobel filter (see the portion inside the red circles).

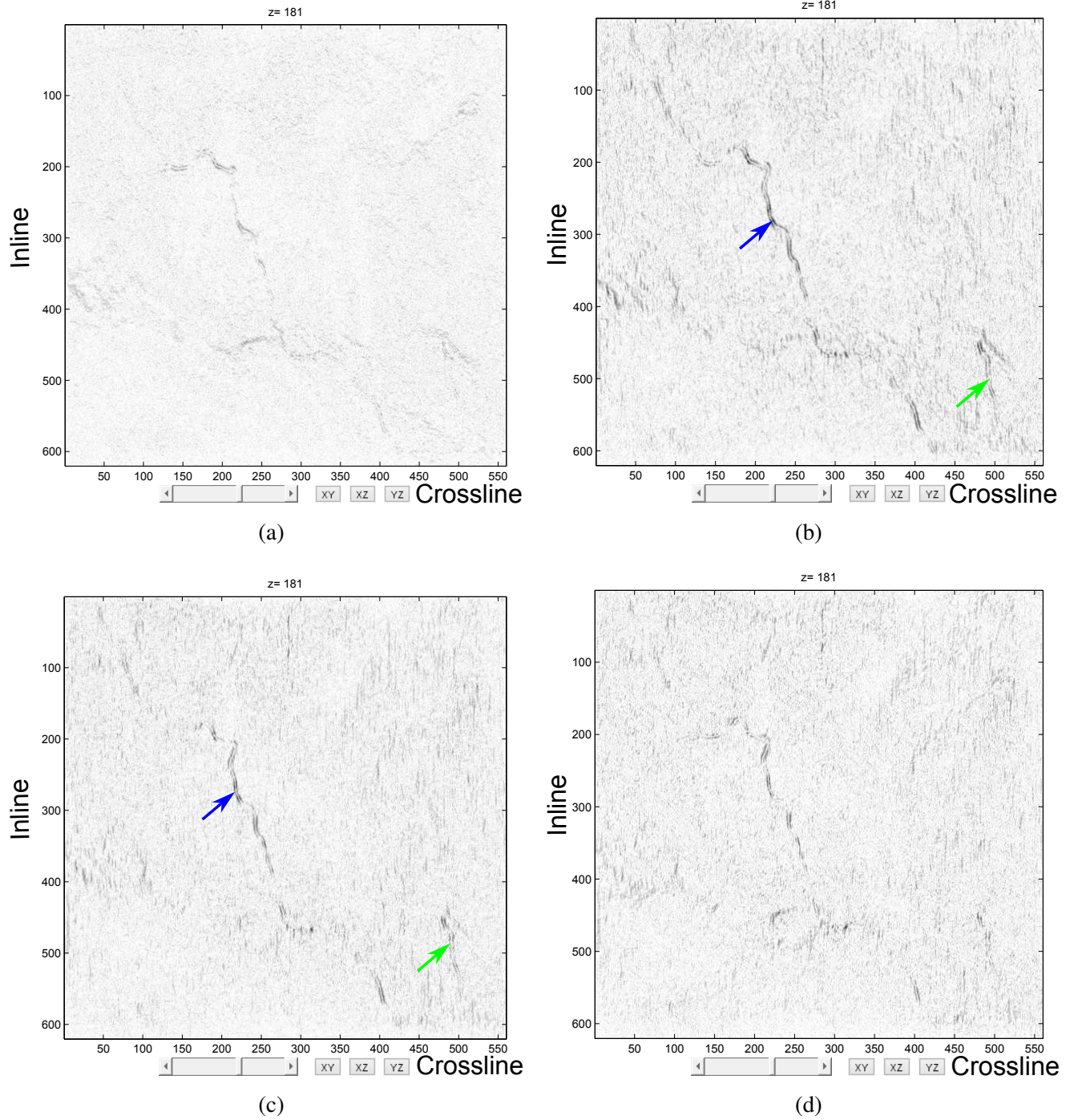
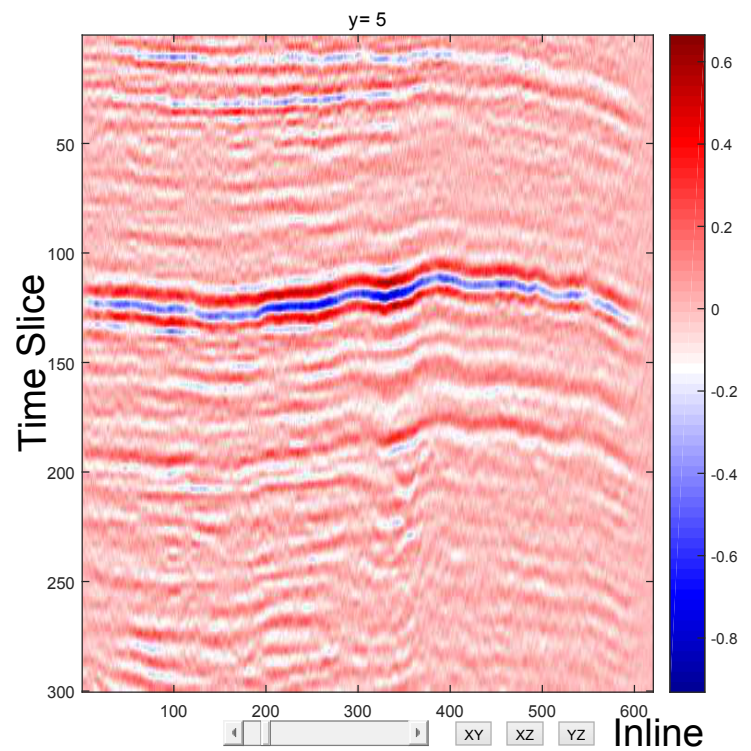
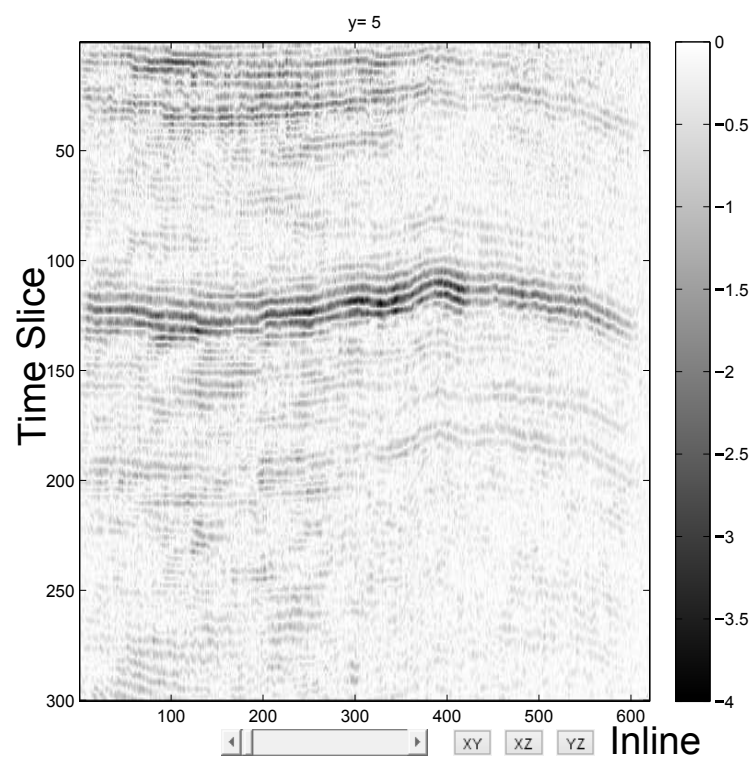


Figure 4.12: Gradient edge maps of 3 x 3 x 3 magic cube  $F_2$  operator using (a) K-5a, (b) K-6a, (c) K-7a and (d) K-8a kernels respectively. The blue and green arrows denote delineated channels.





(a)



(b)

Figure 4.13: Gradient edge maps; (a) Inline number 5 from 3-D seismic volume and (b) Result of the 3 x 3 x 3 magic cube  $F_2$  operator with K-7a.

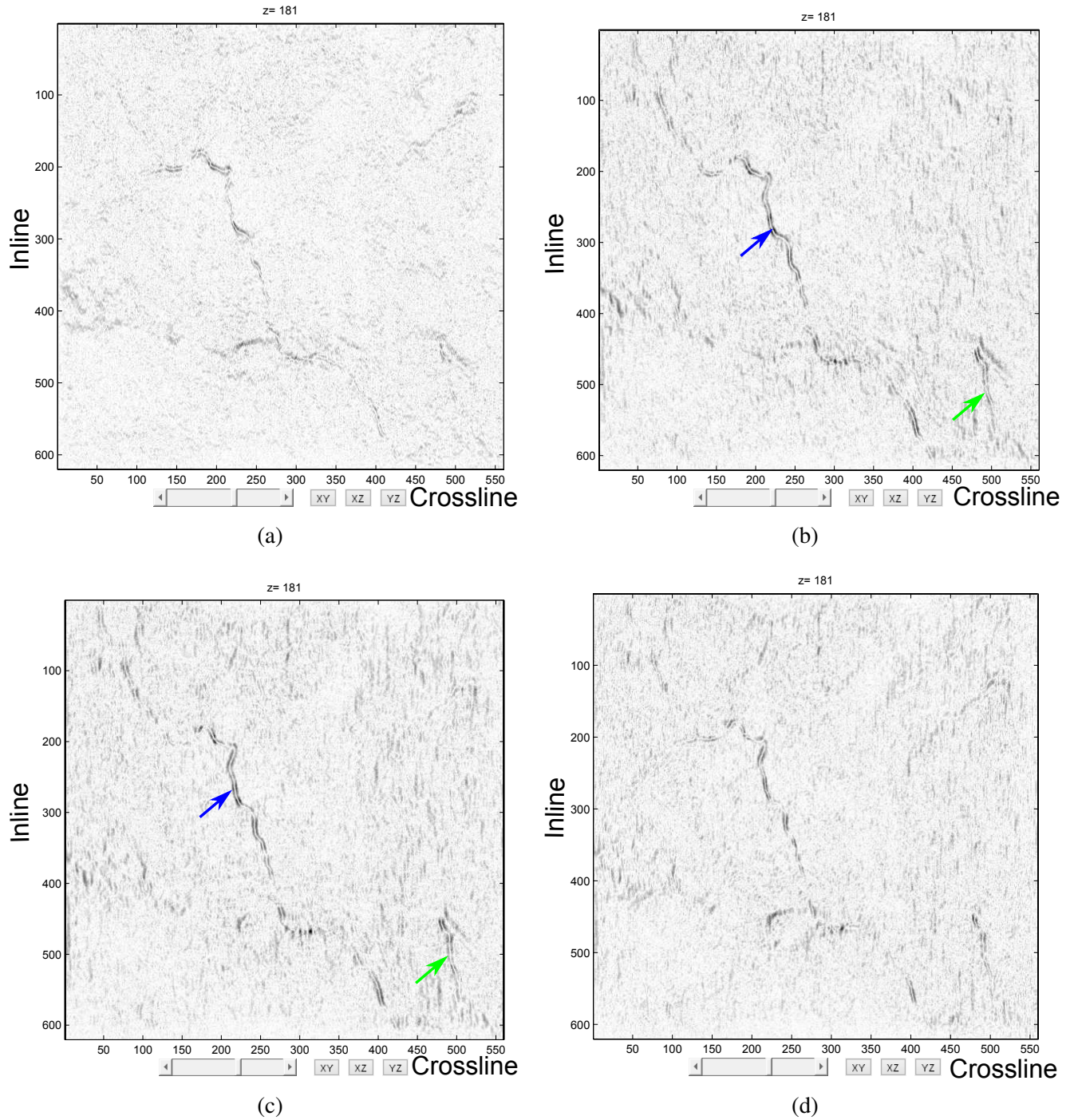
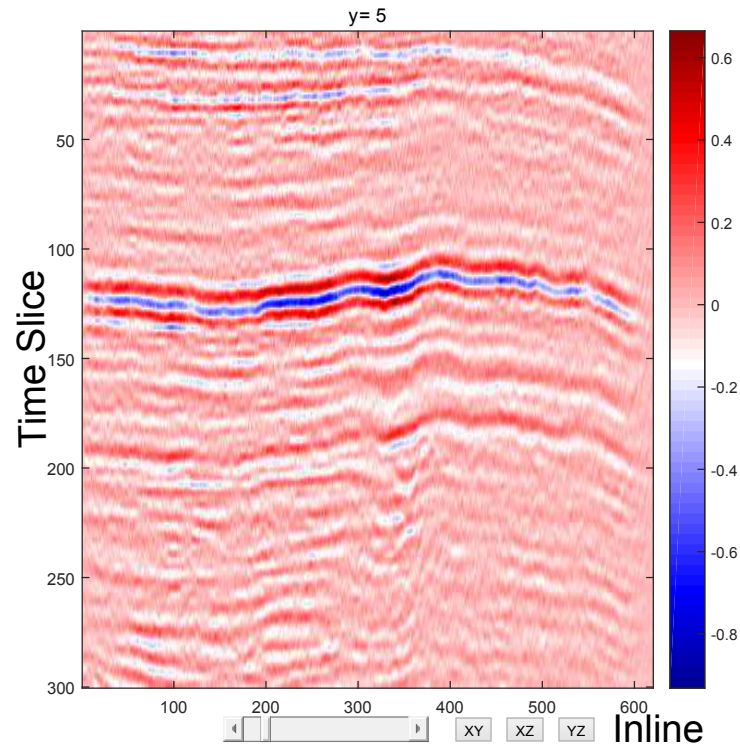
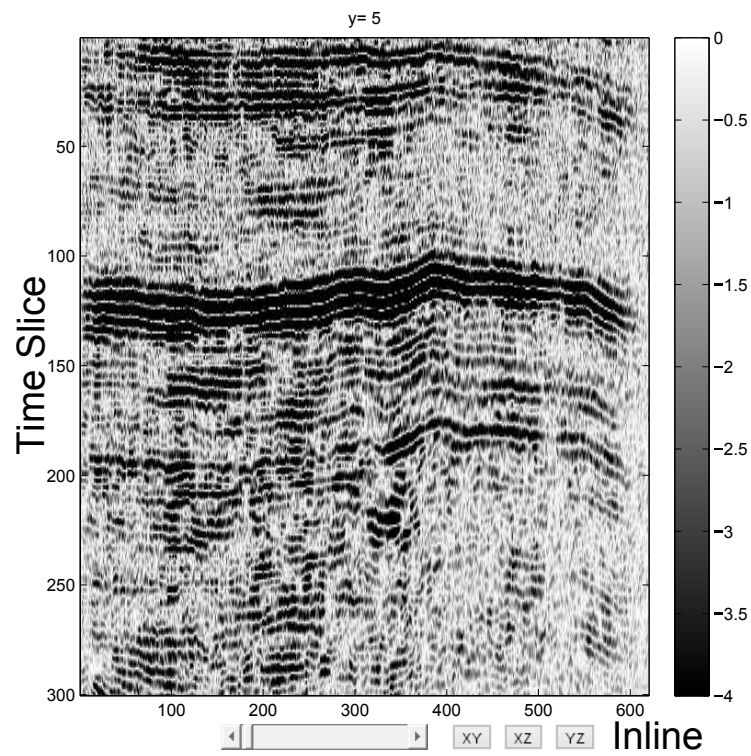


Figure 4.14: Gradient edge maps of 5 x 5 x 5 magic cube  $F_2$  operator using (a) K-5b, (b) K-6b, (c) K-7b and (d) K-8b kernels respectively.



(a)



(b)

Figure 4.15: Gradient edge maps; (a) Inline number 5 from 3-D seismic volume and (b) Result of the 5 x 5 x 5 magic cube  $F_2$  operator with K-7b.



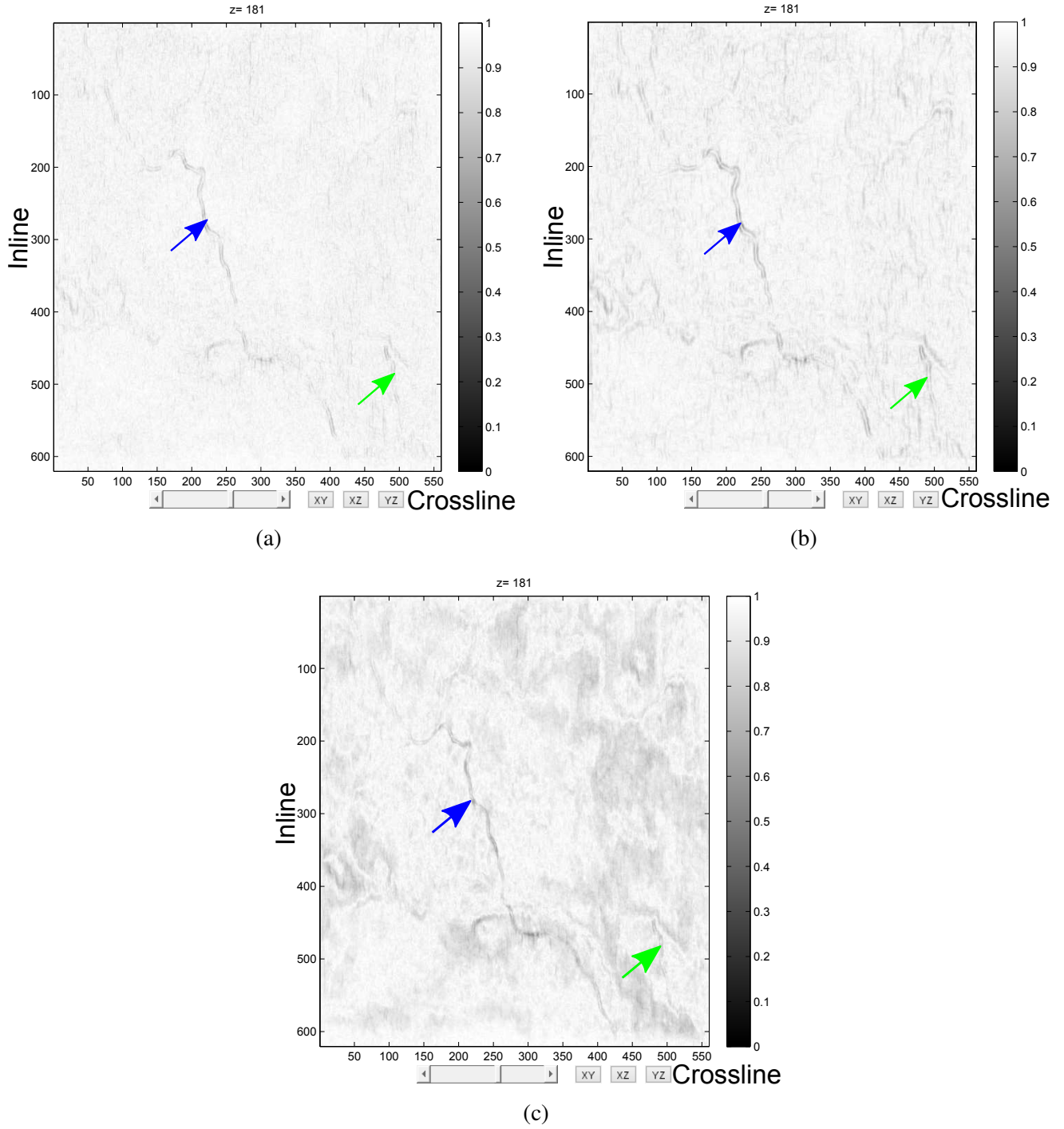


Figure 4.16: Comparison of gradient edge maps of time slice 181; (a) Result of the maximum convolution of  $3 \times 3 \times 3$  magic cube  $F_2$  operators, (b) Result of the maximum convolution of  $5 \times 5 \times 5$  magic cube  $F_2$  operators and (c) Result of 3-D Sobel operator.

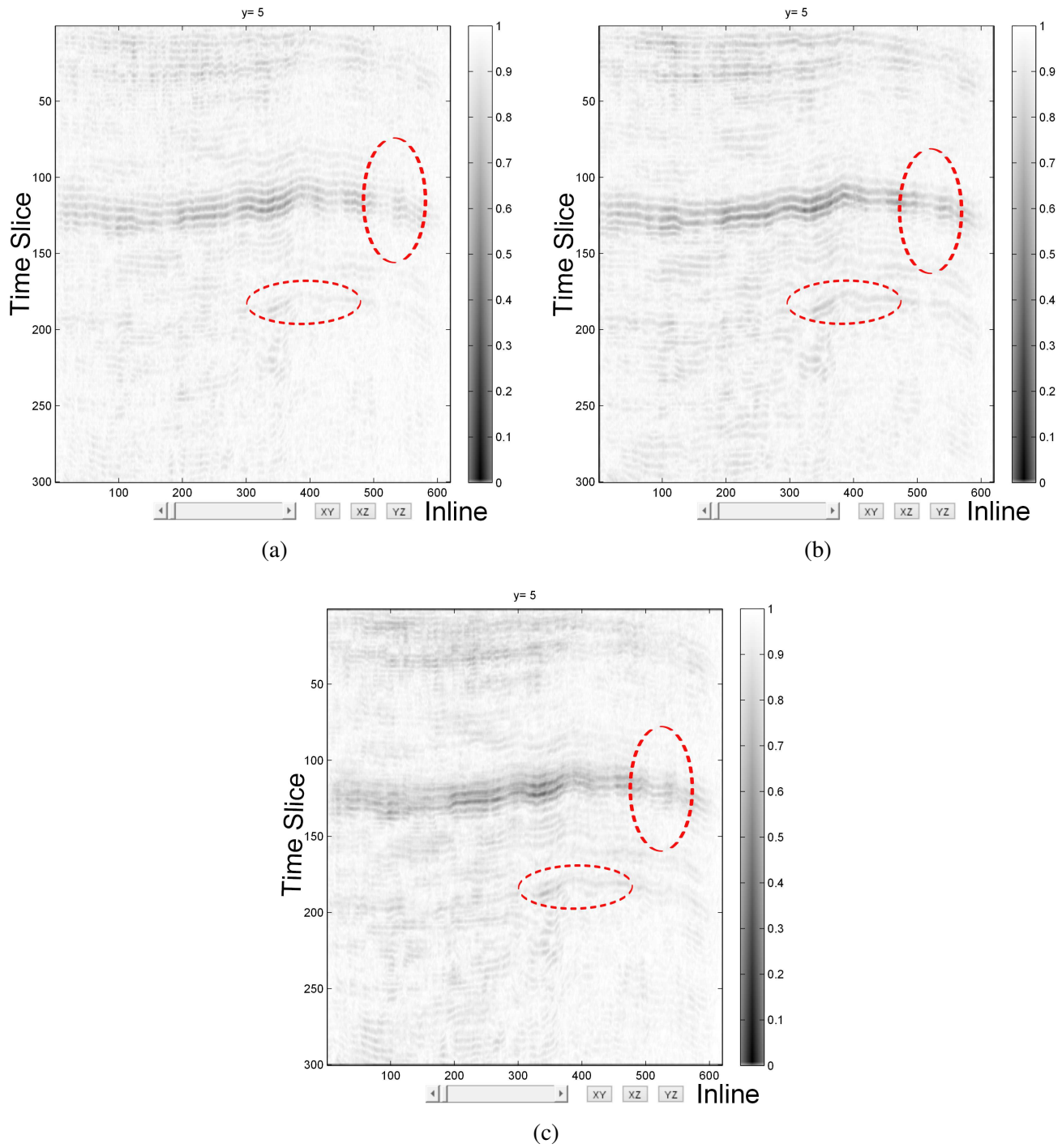


Figure 4.17: Comparison of amplitude gradient edge maps of inline number 5; (a) Result of the maximum convolution of  $3 \times 3 \times 3$  magic cube  $F_2$  operators, (b) Result of the maximum convolution of  $5 \times 5 \times 5$  magic cube  $F_2$  operators and (c) Result of 3-D Sobel operator.

### 4.3 Discussion

The magic square operator is very suited to evaluating amplitude gradients of 2-D seismic data. Each directional kernel is capable of delineating geological features that are perpendicular to its primary direction. Both  $F_1$  and  $F_2$  magic squares clearly locate the two main channels in the data. The result suggests that stratigraphic features (such as channels) in any orientation can be mapped effectively with the magic square operators. The magic square of larger window size shows superior performance over the 3 x 3 magic square operators particularly in the presence of noise. The results of 3 x 3 and 5 x 5 magic square  $F_2$  operators are comparable to that of Sobel in all respects, there is little or no visual observable difference, while 5 x 5 magic square  $F_1$  operators appear slightly better than that of 5 x 5 Sobel operators.

The proposed magic cube operators clearly delineated two channels (indicated by green and blue arrows in Figure 4.12b). The kernels enhanced features perpendicular to their directions. The features are also slightly visible with kernel-7a because it is capable of identifying vertical/near vertical features, and therefore has the advantage to delineate steeply dipping events than the Sobel operator. The 5 x 5 x 5  $F_2$  operators work in a similar fashion. The result is obviously clearer, sharper and crisper. The inline gradient is superb when compared to that of the 3 x 3 x 3. The 5 x 5 x 5  $F_2$  operator produces high amplitude, more continuous and mappable horizons that can easily be followed and interpreted better than in the original inline display.

## CHAPTER 5

# CONCLUSION AND RECOMMENDATIONS

### 5.1 Conclusion

New edge detection methods in both 2-D and 3-D have been presented in this study. The results obtained reveal the operators capability to evaluate and identify discontinuities in seismic data. The magic square  $F_1$  operator averages the full eight separated items corresponding to all rows, columns and diagonals in derived masks. Therefore the image edge gradient map obtained by evaluation of the function is sensitive to small changes in the value of the gradient because it could amplify the magnitude of the gradient of the original amplitude.

In comparison, the  $F_2$  operator is the best choice for edge detection because it scans through the input seismic data in all compass directions which offers the interpreter the

advantage and flexibility to view seismic data in orientations of choice to see certain geologic features of interest at a time among many reflection events. The operators allow the seismic interpreter to see horizontal, vertical and directional features independently that may otherwise have been impossible with other edge detection operators.

The  $5 \times 5$  magic square and  $5 \times 5 \times 5$  magic cube operators involve more neighboring pixel values into the amplitude gradient computation leading to higher quality results and more geological details. Comparing the results of the  $3 \times 3$  with  $5 \times 5$  magic squares as well as  $3 \times 3 \times 3$  with  $5 \times 5 \times 5$  magic cube, we find three main advantages for increasing the spatial analysis window:

- Noise reduction
- Clearer/crisp geologic features detection
- Better directional delineation of geologic features of interest, leading to a better understanding of geologic system.

Hence, the proposed method can be used as a complementary tool in seismic attribute analysis and interpretation. It should however be noted that to get quality output, the input data has to be filtered and denoised using edge preserving smoothing (EPS), median filters, wavelet denoising from wavelet analysis or other algorithms that remove random noise while preserving the inherent masked features of interest.



## 5.2 Recommendations

This study has presented a procedural implementation for the use of magic squares and cubes for edge detection algorithms to map discontinuities in seismic data. Although the results obtained from the operators are good and promising, future work could include the following:

- The example shown in this study contains only channels. In order to test the suitability of the method for mapping structural features like faults, synthetic data incorporating all geological features is recommended. That will enable us to adequately evaluate the limitations and strengths of the method.
- The procedure for computer implementation of the edge detection magic square and cube should be improved to minimize the run time.

# **APPENDIX**

## **THE SOBEL OPERATOR**

## 2-D Sobel

f	g	h
i	j	k
l	m	n

Considering a point (j) on Cartesian grid and its eight neighboring density values as shown above. The directional derivative estimate vector,  $\Delta$ , is defined (Sobel, 1970) as:

$$\Delta = \frac{\text{Density difference}}{\text{Distance to neighbor}} \quad (\text{A-1})$$

The central gradient estimation is a vector sum of a pair of orthogonal vectors (Sobel, 1970). Each orthogonal vector is a directional derivative estimation multiplied by a unit vector specifying the derivative direction, i.e.,

$$\Delta = \frac{h-l}{R} \cdot \frac{[1,1]}{R} + \frac{f-n}{R} \cdot \frac{[-1,1]}{R} + (g-m) \cdot [0,1] + (k-i) \cdot [1,0] \quad (\text{A-2})$$

where  $R = \sqrt{2}$  which represent the distance to neighbor

$$\Delta = \frac{h-l}{\sqrt{2}} \cdot \frac{[1,1]}{\sqrt{2}} + \frac{f-n}{\sqrt{2}} \cdot \frac{[-1,1]}{\sqrt{2}} + (g-m) \cdot [0,1] + (k-i) \cdot [1,0] \quad (\text{A-3})$$

$$\Delta = \left[ \frac{(h-l-f+n)}{2} + k - i, \frac{(h-l+f-n)}{2} + (g-m) \right] \quad (\text{A-4})$$

$$\triangle' = 2\triangle = [h - l - f + n + 2(k - i), (h - l + f - n) + 2(g - m)] \quad (\text{A-5})$$

The weighting function (kernel) is extracted as follows:

1	2	1	-1	0	1
0	0	0	-2	0	2
-1	-2	-1	-1	0	1

$D_x$   
(a)

$D_y$   
(b)

$D_y$  is a 90 degree rotation of  $D_x$ .

### **3-D Sobel**

2-D Sobel filter is extended to 3-D (Al-Dossary and Al-Garni, 2013) as:

$$D_x = \begin{bmatrix} 1 & 1 & 1 \\ 0 & 0 & 0 \\ -1 & -1 & -1 \end{bmatrix} \begin{bmatrix} 1 & 2 & 1 \\ 0 & 0 & 0 \\ -1 & -2 & -1 \end{bmatrix} \begin{bmatrix} 1 & 1 & 1 \\ 0 & 0 & 0 \\ -1 & -1 & -1 \end{bmatrix} \quad (\text{A-6})$$

$$D_y = \begin{bmatrix} 1 & 0 & -1 \\ 1 & 0 & -1 \\ 1 & 0 & -1 \end{bmatrix} \begin{bmatrix} 1 & 0 & -1 \\ 2 & 0 & -2 \\ 1 & 0 & -1 \end{bmatrix} \begin{bmatrix} 1 & 0 & -1 \\ 1 & 0 & -1 \\ 1 & 0 & -1 \end{bmatrix} \quad (\text{A-7})$$

$$D_z = \begin{bmatrix} 1 & 1 & 1 \\ 1 & 2 & 1 \\ 1 & 1 & 1 \end{bmatrix} \begin{bmatrix} 0 & 0 & 0 \\ 0 & 0 & 0 \\ 0 & 0 & 0 \end{bmatrix} \begin{bmatrix} -1 & -1 & -1 \\ -1 & -2 & -1 \\ -1 & -1 & -1 \end{bmatrix} \quad (\text{A-8})$$

The gradients along orthogonal directions are computed by convolving  $D_x$ ,  $D_y$  and  $D_z$  with the input data,  $I(x,y,z)$ , as:

$$\Delta_x(x,y,z) \approx D_x * I(x,y,z) \quad (\text{A-9})$$

$$\Delta_y(x,y,z) \approx D_y * I(x,y,z) \quad (\text{A-10})$$

$$\Delta_z(x,y,z) \approx D_z * I(x,y,z) \quad (\text{A-11})$$

\* means convolution operation

At each point of an image an approximation of the gradient ( $D$ ) is computed by combining the results as follows:

$$D = \sqrt{\Delta_x^2 + \Delta_y^2 + \Delta_z^2} \quad (\text{A-12})$$

# REFERENCES

- Al-Dossary, S., and K. Al-Garni, 2013, Fault detection and characterization using a 3D multidirectional Sobel filter: Presented at the SPE Saudi Arabia Section Technical Symposium and Exhibition, Society of Petroleum Engineers.
- Al-Dossary, S., and K. Marfurt, 2003, Improved 3D seismic edge-detection filter applied to Vinton Dome, Louisiana: 73rd Ann. Internat. Mtg., Soc. of Expl. Geophys., 2370–2372.
- Al-Dossary, S., K. Marfurt, and N. Al-Binhassan, 2003, Comparative study of edge-detection algorithms: 73rd Ann. Internat. Mtg., Soc. of Expl. Geophys., 494–497.
- Al-Dossary, S., K. Marfurt, and Y. Luo, 2002, 3D edge preserving smoothing for seismic edge detection: 72nd Ann. Internat. Mtg, Soc. of Expl. Geophys., 524–527.
- Al-Dossary, S., and K. J. Marfurt, 2006, 3D volumetric multispectral estimates of reflector curvature and rotation: *Geophysics*, **71**, P41–P51.
- Al-Shuhail, A., and S. Al-Dossary, 2014, Two efficient edge detecting operators derived from  $3 \times 3$  magic squares: Presented at the 11th Middle East Geosciences Conference and Exhibition, GEO2014, Bahrain.
- Andrews, W. S., 2004, Magic squares and cubes: Cosimo, Inc.

- Aqrawi, A. A., T. H. Boe, and S. Barros, 2011, Detecting salt domes using a dip guided 3D Sobel seismic attribute: 81st Ann. Internat. Mtg, Soc. of Expl. Geophys., 1014–1018.
- Aydin, T., Y. Yemez, E. Anarim, and B. Sankur, 1996, Multidirectional and multiscale edge detection via m-band wavelet transform: IEEE Transactions on Image Processing, **5**, 1370–1377.
- Bahorich, M., and S. Farmer, 1995, 3-D seismic discontinuity for faults and stratigraphic features: The coherence cube: The Leading Edge, **14**, 1053–1058.
- Benson, W. H., and O. Jacoby, 1976, New recreations with magic squares: Dover Publications.
- Bouvier, J., C. Kaars-Sijpesteijn, D. Kluesner, C. Onyejekwe, and R. Van der Pal, 1989, Three-dimensional seismic interpretation and fault sealing investigations, Nun River Field, Nigeria: AAPG Bulletin, **73**, 1397–1414.
- Boyer, C., 2003, Perfect magic cube: [http://en.wikipedia.org/wiki/Perfect\\_magic\\_cube](http://en.wikipedia.org/wiki/Perfect_magic_cube).
- Brown, A. R., 2001, Understanding seismic attributes: Geophysics, **66**, 47–48.
- Canny, J., 1986, A computational approach to edge detection: IEEE Transactions on Pattern Analysis and Machine Intelligence, **PAMI-8**, 679–698.
- Carron, T., and P. Lambert, 1994, Color edge detector using jointly hue, saturation and intensity: International Conference on Image Processing, IEEE, 977–981.
- Chen, Q., and S. Sidney, 1997, Seismic attribute technology for reservoir forecasting and monitoring: The Leading Edge, **16**, 445–456.

- Chen, X.-H., Z.-H. He, X.-T. Wen, and W.-L. Zhong, 2011, Fracture multi-frequency edge detection based on generalized s transform: *Journal of Jilin University, Earth Science Edition*, **41**, 1605–1609.
- Chen, Z., and S. Nie, 2007, Two efficient edge detecting operators derived from  $3 \times 3$  magic squares: *Proceedings of the International Conference on Wavelet Analysis and Pattern Recognition*, IEEE, 532–534.
- Christensen, N. I., and W. D. Mooney, 1995, Seismic velocity structure and composition of the continental crust: A global view: *Journal of Geophysical Research: Solid Earth* (1978–2012), **100**, 9761–9788.
- Christov, I., 2004, Multiscale image edge detection: 1.130/18.327, Spring 2004, Final Project, May, **12**.
- Di, H., and D. Gao, 2014, Gray-level transformation and canny edge detection for 3D seismic discontinuity enhancement: *Computers & Geosciences*, **72**, 192–200.
- Ecker, C., J. Dvorkin, and A. Nur, 1998, Sediments with gas hydrates: Internal structure from seismic AVO: *Geophysics*, **63**, 1659–1669.
- Gersztenkorn, A., and K. J. Marfurt, 1999, Eigenstructure-based coherence computations as an aid to 3-D structural and stratigraphic mapping: *Geophysics*, **64**, 1468–1479.
- Gonzalez, R., and R. Woods, 2008, *Digital image processing*: Pearson Prentice Hall, NJ.
- Haralick, R. M., 1984, Digital step edges from zero crossing of second directional derivatives: *IEEE Transactions on Pattern Analysis and Machine Intelligence*, 58–



68.

Haralick, R. M., S. R. Sternberg, and X. Zhuang, 1987, Image analysis using mathematical morphology: IEEE Transactions on Pattern Analysis and Machine Intelligence, 532–550.

Heinz, H. D., and J. R. Hendricks, 2000, Magic square lexicon: Illustrated: HDH.

Hellmich, C., and H. Trappe, 1998, Carboniferous Case Study - Combining 3D Seismic Inversion and 3D Heterogeneity Results for Optimal Well and Production Planning: 60th Mtg., Eur. Assn. Geosci. Eng., Session:W502.

Hesthammer, J., and H. Fossen, 1997, Seismic attribute analysis in structural interpretation of the gulfaks field, northern north sea: Petroleum Geoscience, **3**, 13–26.

Iske, A., and T. Randen, 2005, Methods and modelling in hydrocarbon exploration and production: Springer.

Jing, Z., Z. Yanqing, C. Zhigang, and L. Jianhua, 2007, Detecting boundary of salt dome in seismic data with edge detection technique: 77th Ann. Internat. Mtg, Soc. of Expl. Geophys., 1392–1396.

Julesz, B., 1959, A method of coding television signals based on edge detection: Bell System Technical Journal, **38**, 1001–1020.

Jurado, M., and M. Comas, 1992, Well log interpretation and seismic character of the cenozoic sequence in the northern alboran sea: Geo-Marine Letters, **12**, 129–136.

Justice, J., D. Hawkins, and G. Wong, 1985, Multidimensional attribute analysis and pattern recognition for seismic interpretation: Pattern Recognition, **18**, 391–399.

Lee, J.-S., Y.-N. Sun, and C.-H. Chen, 1995, Multiscale corner detection by using

- wavelet transform: Image Processing, IEEE Transactions on, **4**, 100–104.
- Lisle, R. J., 1994, Detection of zones of abnormal strains in structures using gaussian curvature analysis: AAPG bulletin, **78**, 1811–1819.
- Loly, P., I. Cameron, W. Trump, and D. Schindel, 2009, Magic square spectra: Linear Algebra and its Applications, **430**, 2659–2680.
- Luo, Y., W. G. Higgs, and W. S. Kowalik, 1996, Edge detection and stratigraphic analysis using 3-D seismic data: 66th Ann. Internat. Mtg, Soc. of Expl. Geophys., 324–327.
- Marques, O., 2011, Practical image and video processing using matlab: John Wiley & Sons.
- Marr, D., and E. Hildreth, 1980, Theory of edge detection: Proceedings of the Royal Society of London. Series B. Biological Sciences, **207**, 187–217.
- Matheron, G., 1965, Axiomatique des milieux poreux aléatoires: The Library of the Ecoledes Mines de Paris.
- Matheron, G., and J. Serra, 2002, The birth of mathematical morphology: Mathematical morphology, 1–50.
- Meldahl, P., R. Heggland, B. Bril, and P. de Groot, 2001, Identifying faults and gas chimneys using multiattributes and neural networks: The Leading Edge, **20**, 474–482.
- Ollerenshaw, D. K., and D. S. Brée, 1998, Most-perfect pandiagonal magic squares: their construction and enumeration: Institute of Mathematics and its Applications.
- Pampanelli, P. C. P., P. M. Silva, and M. Gattass, 2013, A new volumetric fault at-

- tribute based on first order directional derivatives: 13th International Congress of the Brazilian Geophysical Society, Rio de Janeiro, Brazil, Brazilian Geophysical Society, 1621–1625.
- Pepper, R. E., and P. P. Van Bemmelen, 2000, Seismic signal processing method and apparatus for generating a cube of variance values. (US Patent 6,151,555).
- Prewitt, J. M., 1970, Object enhancement and extraction: Picture processing and Psychopictorics, **10**, 15–19.
- Randen, T., S. Pedersen, and L. Sonneland, 2001, Automatic extraction of fault surfaces from three-dimensional seismic data: 71st Ann. Internat. Mtg, Soc. of Expl. Geophys., 551–554.
- Roberts, L. G., 1963, Machine perception of three-dimensional shapes: PhD thesis, Massachusetts Institute of Technology, USA.
- Ruzon, M. A., and C. Tomasi, 1999, Color edge detection with the compass operator: Presented at the Conference on Computer Vision and Pattern Recognition: Computer Society, IEEE.
- Sangree, J., and J. Widmier, 1978, Seismic stratigraphy and global changes of sea level, part 9: Seismic interpretation of clastic depositional facies: AAPG Bulletin, **62**, 752–771.
- Semanišinová, I., and M. Trenkler, 2007, Discovering the magic of magic squares: The Mathematics Teacher, **101**, 32–39.
- Sertcelik, I., and O. Kafadar, 2012, Application of edge detection to potential field data using eigenvalue analysis of structure tensor: Journal of Applied Geophysics, **84**,

86–94.

- Sharifi, M., M. Fathy, and M. Tayefeh Mahmoudi, 2002, A classified and comparative study of edge detection algorithms: Proceedings of International Conference on Information Technology: Coding and Computing, IEEE, 117–120.
- Skirius, C., S. Nissen, N. Haskell, K. Marfurt, S. Hadley, D. Ternes, K. Michel, I. Reglar, D. D’Amico, F. Deliencourt, T. Romero, R. D’Angelo, and B. Brown, 1999, 3-D seismic attributes applied to carbonates: The Leading Edge, **18**, 384–393.
- Sobel, I., 1970, Camera models and machine perception: Technical report, DTIC Document.
- Song, J., X. Mu, Z. Li, C. Wang, Y. Sun, and M. Imran, 2014, Fault identification using dip-guided facet model edge detector: Interpretation, **2**, T89–T101.
- Stright, L., A. Bernhardt, A. Boucher, T. Mukerji, and R. Derksen, 2009, Revisiting the use of seismic attributes as soft data for subseismic facies prediction: Proportions versus probabilities: The Leading Edge, **28**, 1460–1468.
- Sun, J., D. Gu, Y. Chen, and S. Zhang, 2004, A multiscale edge detection algorithm based on wavelet domain vector hidden markov tree model: Pattern Recognition, **37**, 1315–1324.
- Taner, M. T., J. S. Schuelke, R. O’Doherty, and E. Baysal, 1994, Seismic attributes revisited: 64th Ann. Internat. Mtg, Soc. of Expl. Geophys., 1104–1106.
- Tertois, A., and T. Frank, 2004, Data filtering by 3D convolution: Presented at the 24th Gocad Meeting, Gocad.
- Walls, J. D., M. T. Taner, T. Guidish, G. Taylor, D. Dumas, and N. Derzhi, 1999,

North sea reservoir characterization using rock physics, seismic attributes, and neural networks; a case history: 69th Ann. Internat. Mtg, Soc. of Expl. Geophys., 1572–1575.

Woodhall, M., and C. S. Lindquist, 1997, New edge detection algorithms based on adaptive estimation filters: Conference on Signals, Systems & Computers, IEEE, 1695–1699.